The evolution of a turbidite- channel and levees related to the flow dynamics of high-density turbidity currents; Results from flume experiments.

Universiteit Utrecht

Martijn ter Braack
University Utrecht

Table of contents

Abstract

The flow dynamics of turbidity currents in relation to the resulting channel/levee morphology is still poorly understood. In a series of 3D flume experiments the evolution of a turbidite system will be studied in relation with the flow dynamics of high-density turbidity currents. These experiments were carried out in the Eurotank laboratory at the Utrecht University. During the execution of the flume experiments the boundary parameters (concentration, sediment composition, discharge and slope gradient) were varied to explore which boundary settings are necessary to successfully simulate a turbidity system in the laboratory. Velocity profiles were obtained from the turbidity current during the experiment. Deposits were measured with a laser in order to study the morphology of channel and levees and to create digital elevation models of the deposits.

The results of the flume experiments show some similarities with natural turbidite systems but also some fundamental differences are present between overall sediment composition, sediment input orientation and lobe deposits. In future experiments these should be incorporated in order to achieve more realistic results. The results of the velocity profiles and laser scans conclude that confinement of the current is the main factor causing decreasing velocities outside the channel. An increasing channel gradient is the main factor causing increasing velocities inside the channel. Channel formation was initiated by deposition which lead to channelization of the turbidity current and formation of a channel with accompanying levees. After channelization of the flow, velocities in the channel increase and incision in the channel increases. This leads to the transition from an depositional system towards an erosional/depositional system. The turbidite system created in this study started as a depositional system. This is in contradiction with suggestions of Maier et al. (2013) and others (e.g. Campion et al., 2000; Gardner & Borer, 2000; Schwarz & Arnott, 2007; McHarue et al., 2011) which state that such systems do not exist. Results of the backslope of one of the levees are in good agreement with previous flume experiments and natural turbidite systems.

Introduction

One of the most common types of sedimentary rocks are beds deposited from turbidity currents, also called turbidites. They consist out of sands and clays, and may be of siliciclastic or other composition. The early history of the concept of turbidity currents has been reviewed by Walker (1973) and goes back to the mid-thirties (e.g. Daly, 1936). However, it was the experimental and field observations of Philip Kuenen (Kuenen, 1966) which convinced geologists of the existence of turbidity currents (Middleton, 1993). Submarine channels, which cover large sections of the oceans floor, are thought to be formed by these turbidity currents. Currents passing through these channels reshape the morphology of the channels by erosion and deposition, the currents even have effect on the morphology outside the channel. Due to over spilling of the current over the edges of the channel, and deposition of its sediment on the overbanks, levees are created on both sides of the channel.

Although turbidity currents have been studied for quite some time they are still not fully understood. Especially the flow dynamics of turbidity currents in relation with the morphodynamic evolution of channel/levee systems is poorly understood. Understanding the flow dynamics and its relation to the build-up of channels and levees is however fundamental in understanding the deposits formed by turbidity currents. These channel- and levee deposits, and the processes responsible for their architecture, formation, composition and internal structures, are interesting aspects for the hydrocarbon industry. These deposits are potential hydrocarbon reservoirs, and a better understanding of the processes is a vital part in improving the predictive 3D-models used in the hydrocarbon industry.

Turbidite research

There are four main approaches to study turbidity currents: In-situ measurements (Xu et al., 2004), describing turbidite deposits from the geological record, numerical modelling and physical flume experiments. However, not all methods are suitable for studying the dynamics of a turbidity current. Due to the catastrophic nature of a turbidity current it is very difficult to make in-situ measurements. Turbidite deposits from the geological record lack the connection with the dynamics of the current which formed them, although this might be possible in combination with numerical modelling (Pirmez & Imran, 2003). Therefore, the best way to get a better understanding on flow dynamics, and flow dynamics related to the morphological evolution of channels and levees, is by means of numerical modelling and flume experiments.

This study

The aim of this study is to get a better understanding of the evolution of a turbidite channel, its levees and dimensions in relation with the flow dynamics of high-density turbidity currents. This will be done by means of physical flume experiments in which UVP (ultrasonic velocity profile) data and deposit dimensions will be measured. Velocity profiles will be measured in the channel, at the levees and outside the levees. Aspects of the geometry that will be studied are channel width, channel depth, levee height and slope gradient. This will give insight in the processes of confinement, incision, velocity patterns and levee evolution. To achieve this, a series of 3D flume experiments will be conducted in which the boundary parameters (discharge, slope gradient, sediment composition and concentration) will be varied. The results of the 3D tank experiments are compared to natural channel/levee systems to determine to which type of system the results can be compared with. This is done with the database D-MAKS (Deep-Marine Architecture Knowledge Store; Baas et al., 2005) of the Turbidity Research Group, which is based at Leeds University (UK). This database provides a quantitative method for the comparison of deep-marine clastic depositional systems and the analysis of their architectural properties. The database consists out of literature-derived information from ancient and modern surface and sub-surface deep-water system hosted in a relational database comprising 208 systems.

Background

Flow structure and anatomy

Figure 1 shows a simplified sketch of a turbidity current (Meiburg & Kneller, 2010). A turbidity current can be subdivided into a head (front), body and tail (Middleton, 1966a,b & Simpson, 1987). The head and body of the flow can be connected by a neck. The head and neck are considered unstable and are characterized by a high amount of turbulence and fluctuating velocities. The body of the flow also shows significant turbulence, but over a longer time interval the conditions in the body are considered stable (in average). There are three resisting forces acting on the head: the ambient fluid resistance, the bed friction and the upper interface friction. Due to the bed friction a 'nose' shape is established at the front of the head, and due to shearing at the top of the head, with the ambient fluid, turbulent mixing is created at the back of the head (Middleton, 1993). Because the head experiences sufficient resistance from the ambient fluid, flow velocities are highest in the body (Leeder, 1999; Meiburg & Kneller, 2010). This difference in velocity may be associated with a hydraulic jump and changes in flow properties. Because the head is held back by the ambient fluid its velocity is largely independent from changes in the gradient of the slope of the bedding plain. This gradient plays a major role for the velocity of the body of the current.

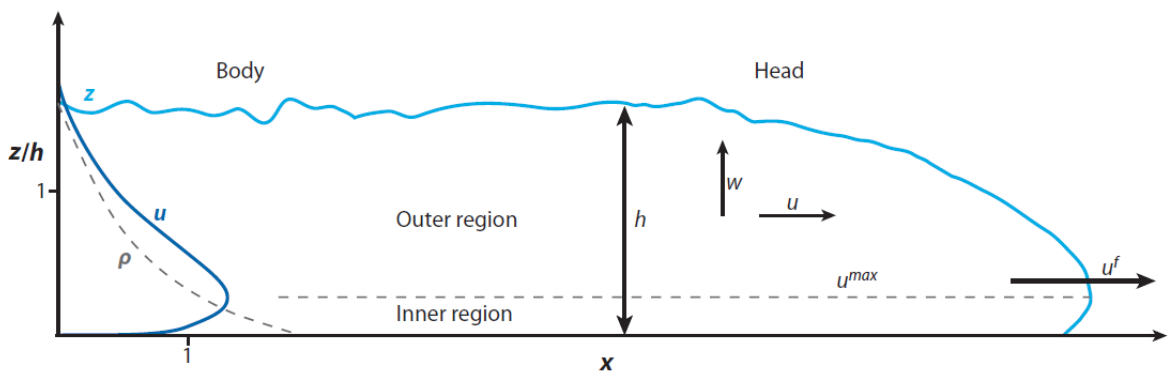

Figure 1: Simplified sketch of a turbidity current showing a velocity- and density profile (Meiburg & Kneller, 2010)

Methods

Experimental set up

3D Tank

Experiments in the 3D tank we conducted in the Eurotank Flume Labaratory at Utrecht University. The 3D flume is 6 m wide, 11 m long and 1.2 m deep (fig. 2). Within the tank a continental-slope/abyssal plain relief was created. This relief was covered with a sand mixture of 2(129 µm):3(146 µm):1(210 µm):1(267 µm) which formed the (erodible) sea bed. The slope was varied between 10-12° and its length was ± 4.5 m. At the boundary between the slope and the abyssal plain a height difference of 0.1 m was created. This was done to prevent back-stepping of the lobe, which is deposited on the abyssal plain, onto the slope. Back-stepping of the lobe could result in a disturbance of channel and levee formation on the slope and was therefore prevented. An inlet box was placed at the top of the slope at an angle of approximately 8° and was partly buried within the slope. This box was designed for an equal spreading of the inflow and a gradual spreading of the flow onto the slope by means of unfolding sidewalls. The box was 1.5 m long, 1 m wide and 0.15 m high. After the tank was filled with water a sand mixture was pumped into the tank. The sand mixture was mixed in a 1 m^3 mixing tank, which was designed to homogenise sand-water mixtures up to a concentration of 30%. The mixture was pumped through a pipeline with a discharge meter (Krohne Optiflux 2003) towards the inlet box. The pipeline was cleared of air and filled with water prior to the start of the experiment to reduce unnecessary entrapment of air.

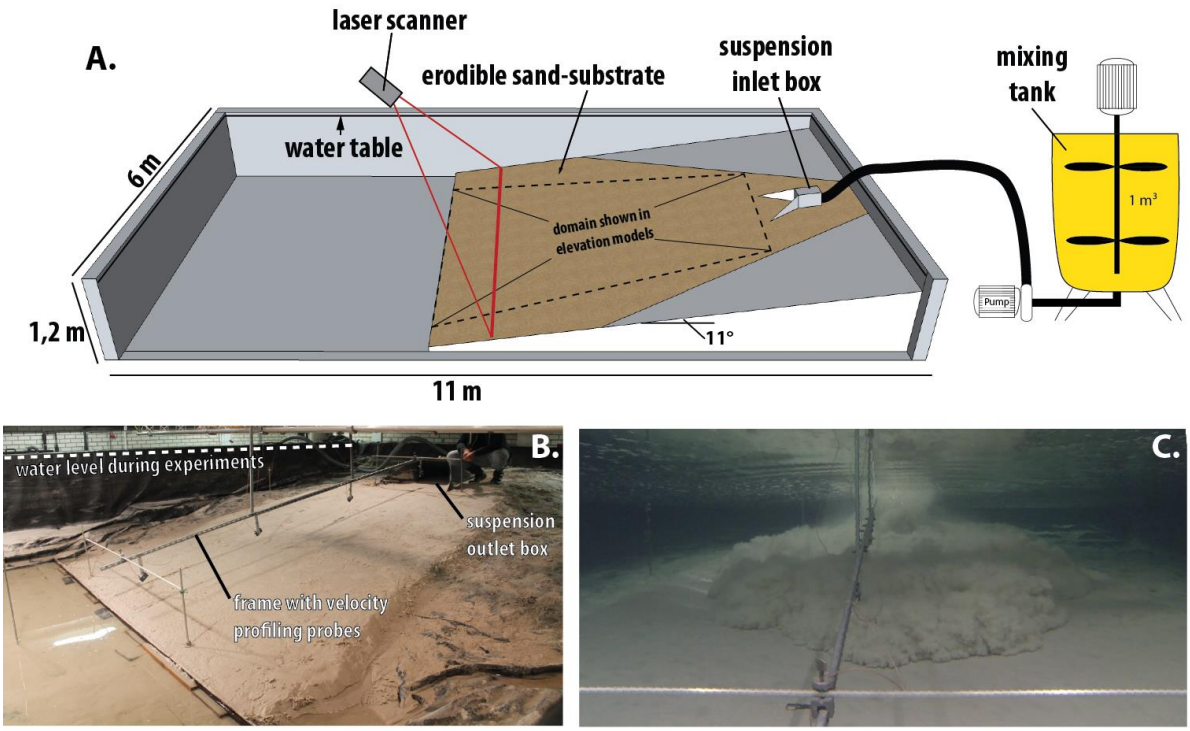

Figure 2: (a) Schematic overview of the set up used during the 3D flume experiments. (b) Drained tank prior to an experiment. (c) Underwater view showing a turbidity current flowing down slope during an experiment.

Four UVP-probes were used to measure velocities and turbulence of the flow. These probes were used in two different measuring set ups. In the first set up the probes were placed along the slope, aligned with each other (fig. 2b). They were aligned to the centre of the inlet box and spaced 1.3 m from each other, with the first probe positioned at the inlet box were the flow enters the tank and the last probe positioned at the end of the slope. The probes were placed at an angle of 60° with the slope and at a height of 0.13 m with the bed. This was done to measure changes in horizontal velocities as the turbidity current flows down the slope. In the second set up four probes and an additional probe were used. The probes were placed next to each other at a fixed distance on the slope (4.45 m from the front of the tank). The probes were spaced 0.25 m from each other with an angle of 60° with the bed, and at a height of 0.13 m from the bed. The first probe was placed above the left levee, the second probe was placed above the centre of the channel, the third probe was placed above the right levee and the fourth probe was placed at the right side of the right levee above the slope. These probes were used to measure the horizontal velocity down the slope (probe points towards the turbidity current). The additional probe was used to measure the horizontal velocity to the edge of the slope (probe points towards the side of the turbidity current). This probe was placed as closely as possible to the third probe, also with an angle of 60° and at a height of 0.13 m from the bed. This set up was used in order to determine the change in down slope velocity towards the edge of the slope and to measure the sideway velocity (spreading) of the turbidity current as it flows down the slope.

The morphology of the slope was measured with a horizontal resolution of 2x2 mm prior and after an experiment with a laser scanner (fig. 2b. This was done in order to accurately measure the difference in morphology before and after each experiment.

Grain size distribution

Figure 3 shows the distribution of the grain particles (D50) used in the experiments of this study. Aim of this study was to create a HDTC existing only out of sand particles. Grain sizes, which were used, have been picked for a smooth transition from fine fraction to coarser fractions, without big gaps between grain sizes.

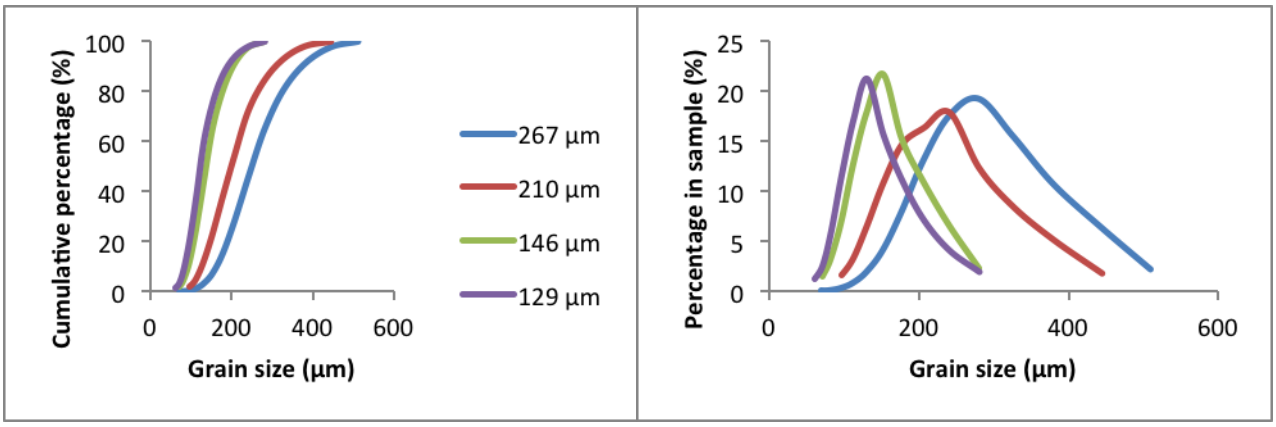

Figure 3: Grain size (D50) distribution of the sediments used in this study.

corrected for the measuring angle of the probe. This can be calculated with a straight-forward angle correction, assuming that the bulk of the turbidity current moves parallel to the bedding plane and vertical movement is only due to turbulence which results in no net movement. The velocity of the incoming turbidity current can be translated to a vector X. With the angle of the probe (α = 60°) and the velocity data obtained, velocity vector X can be calculated. In order to obtain a vertical velocity profile the data has to be averaged over a certain time interval. This average has been taken from the body of the turbidity current, as conditions in the body are assumed to be steady.

Calculating velocity profiles and values

From the velocity data single values are calculated to simplify analytical work and for the calculation of dimensionless parameters and other parameters. From the velocity data the maximum velocity (U_{max}) and the depth average velocity (U_{mean}) are obtained. U_{max} is measured for every time step of the probes (0.55 sec) over the entire time duration of each run.

U_{mean} is calculated over the entire length of the velocity profile. There are however some problems which have to be taken into account when calculating the mean velocity. First of all the shifting of the bedding plane due to aggradation/erosion over time, meaning that the total distance over which the mean velocity is calculated has to be changed over time. Shifting of the bedding plain can also cause the top region of the current to reach above the probe. Also not all velocity profiles show a curve that reaches zero velocity at the bed, which means that the mean velocity can be overestimated.

Digital elevation model (DEM) and cross-sections

The data obtained from the laser is used to create digital elevation models (DEM) of the experiments. These models show the difference in deposition between the executed experiment and the initial slope prior to the experiment. From the DEM's, cross-sections of the channel and levees are made over the entire length of the slope. From these cross-sections all sorts of information can be deduced such as levee elevation, channel depth, channel width, deposition rates and other parameters.

Dimensionless scaling

Because the experiments carried out in this study are on a different scale than natural occurring turbidity currents, it is important to check whether the experiments carried out here are still comparable to the natural processes. This is done by means of dimensionless parameters such as the Froude number and Reynolds number. The Froude number is given by the following equation:

$$Fr' = \frac{U}{\sqrt{g'H}}\ [-] \qquad (1)$$

In which U stands for the depth-averaged flow velocity, H for the flow height and g for the gravitational acceleration.

The Reynolds number is used as an indicator for turbulence. The Reynolds number should be >2000 for turbulent conditions in our experiments. The Reynolds number is determined by the following equation:

$$Re = \frac{\rho\, U\, H}{\mu}\ [-] \qquad (2)$$

In which ρ stands for the depth-averaged flow density, U for the flow velocity, H for the flow height and μ stands for the dynamic viscosity. No corrections were made for the concentration dependence of the viscosity. A constant viscosity of $1.1 \cdot 10^{-3}$ kg m^{-1} sec^{-1} was assumed.

The paragraph below describes the method used to estimate the depth-averaged velocity (U) and flow height (H) using the "integral method" of parker et al. (1987). This method requires that a velocity and a concentration profile are available. The velocity profiles are present for all runs, however no concentration profiles are available. Therefore 2 estimations of the concentration have been used; method 1) The initial input sediment concentration is used; method 2) 75% of the initial

concentration is used as an estimate based on average concentrations vs. initial concentrations in a series of 2D experiments, also carried out in the Eurotank laboratory in Utrecht (P. Michielsen, 2014).

First, the products Uh, U^2H and UρH are determined:

$$UH = \int_0^\infty u dz \qquad (4)$$

$$U^2H = \int_0^\infty u^2 dz \qquad (5)$$

$$U\rho\mathrm{H} = \int_0^\infty u\rho\, dz \qquad (6)$$

Second, U and h are determined by dividing the outcomes of 4 and 5:

$$U = \frac{U^2H}{UH} \qquad (7)$$

$$H = \frac{UH}{U} \qquad (8)$$

$$\rho = \frac{U\rho\mathrm{H}}{\mathrm{UH}} \qquad (9)$$

Finally, the outcomes of 7,8 and 9 can be used to calculate the Froude and Reynolds number using equation 1 and 2.

Results of flow parameter calculations can be found in table 1.

*Table 1: Flow parameters of all experiments. * method 1; ** method 2.*

Run	U (m/s)	H (m)	ρ (kg/m3)	Fr' *	Fr' **	Re *	Re **
41	0,32	0,039	1,0851	1,21	1,36	13587	12972
42	0,48	0,113	1,026	1,07	1,21	59767	57111
43	0,6	0,079	1,0701	1,62	1,83	52602	50265
44	0,35	0,095		0,77	0,86	31304	29977
45	0,41	0,086	1,0371	0,75	0,84	32966	31473
46	0,49	0,082	1,0481	1,28	1,43	44454	42019
47	0,53	0,075	1,0465	1,26	1,42	42714	40397
48	0,63	0,08	1,0445	1,52	1,71	58490	55302
49	0,55	0,058	1,048	1,54	1,72	36922	34873
50	0,59	0,064	1,0484	1,6	1,8	44245	41845
51	0,7	0,074	1,0568	1,74	1,95	60104	56766

Results

3D Experiments

A total of 11 experiments were executed in which the main objective was to achieve channel and levee formation over the entire length of the slope. To achieve this goal some parameters where modified after an experiment was carried out to improve the next experiment. These parameters are: slope (gradient), discharge, gradient of the inlet box, concentration of the mixture and composition of the mixture. Discharge was varied between 50 m^3/h, 45 m^3/h and 30 m^3/h (± 3 m^3/h). Concentration levels of the mixture were varied between 13% and 17% (± 3%). The composition of the mixture was varied between a ratio of 2[129 µm]:3[146 µm]:1[210 µm]:1[267 µm] and a ratio of 1[129 µm]:1[146 µm]. The experiments can be divided into two parts. In the first part, parameters were constantly changed to improve future experiments. After each experiment was measured, turbidite channels and deposits (levees, lobes) were removed and the slope was restored to its original setting. In between experiments the parameters could be adjusted. In the second part, when the parameters were optimized, three experiments were executed without removing the deposits or restoring the slope. This was done in order to achieve a steady state of channel formation on the slope.

Seven of the 11 experiments were unsuccessful and 4 are considered successful. All runs are summarized in table 2 with their initial parameters. Runs which are considered successful formed a morphology that resembled a leveed channel, unsuccessful runs do not show some sort of channel formation or any morphology which can be related to channel/levee formation. Figures of the deposits of these unsuccessful runs, scanned with the laser, can be found in appendix A, here only the results of the successful runs will be given.

Table 2: Experimental boundary parameters

Run	Con (%)	Comp. (µm) *	Discharge (m^3/h)	Slope gradient (°)
41	13,4	2:3:1:1	20	10
42	13,1	2:3:1:1	50	10
43	13,1	2:3:1:1	45	10
44	13,3	2:3:1:1	50	11
45	13,4	2:3:1:1	50	12
46	17	2:3:1:1	50	12
47	16,8	1:1:0:0	45	12
48	16,9	1:1:0:0	33	12
49	17,3	1:1:0:0	30	12
50	16,8	1:1:0:0	30	12
51	17,4	1:1:0:0	30	12

Successful
Unsuccessful

Run 44

Figure 4 shows the digital elevation model (DEM) of run 44. The initial parameters used for run 44 are listed in table 2.

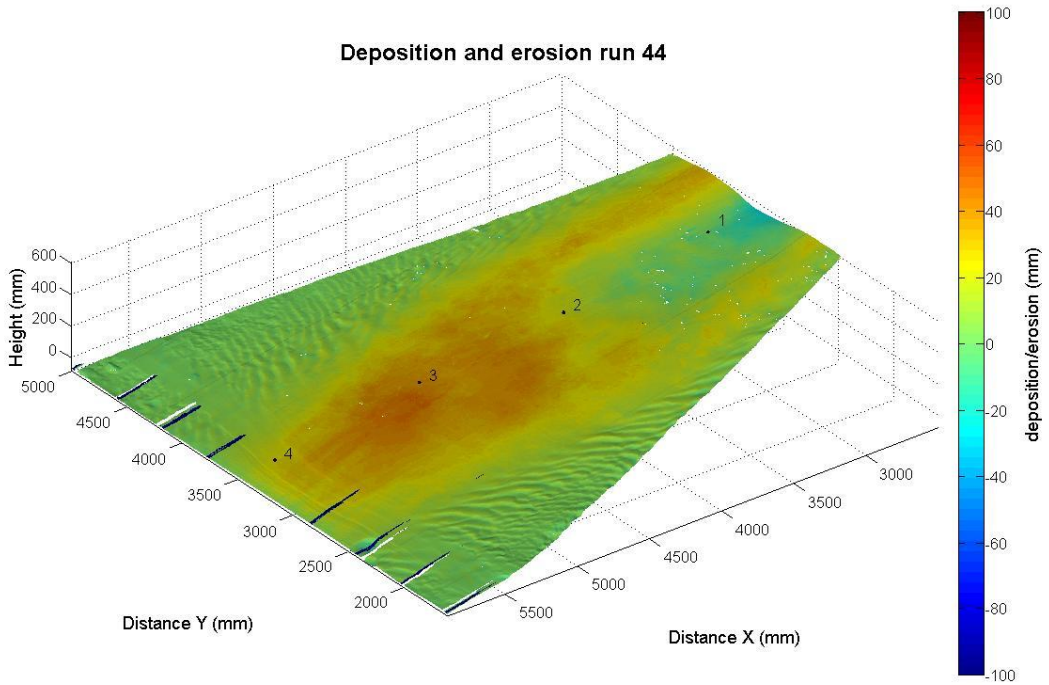

Figure 4: DEM run 44

Deposition is indicated by the yellow to red colours, erosion is indicated by the light blue to dark blue colour. A distinctive feature in the elevation model is the blue spot at the upper boundary of the slope. This area of erosion is caused by the formation of a scour by the turbidity current as it passes the boundary between the inlet box (PVC material) and the slope (sand). Also well visible is the lobe deposited onto the slope and the levees deposited in between the lobe and the upper boundary of the slope, in between the levees a small channel was formed.

Figure 5 shows the velocity data obtained by the UVP probes of run 44.

Additional information regarding velocity profiles (for interpretation)

Velocity data obtained by the probes show a 'spike-like' profile. These spikes are actually turbulence clouds formed at the upper boundary of the turbidity current and are illustrated as spikes due to compression of the x-axis. The head of the turbidity current (left side) is well visible as a high and broad spike. The tail is also well visible at the right side of the profile, where the velocity fades away. The probe positioned in front of the inlet box and shows high, fluctuating velocities, which can be related to the high amount of air trapped within the flow which is released when the flow enters the tank.

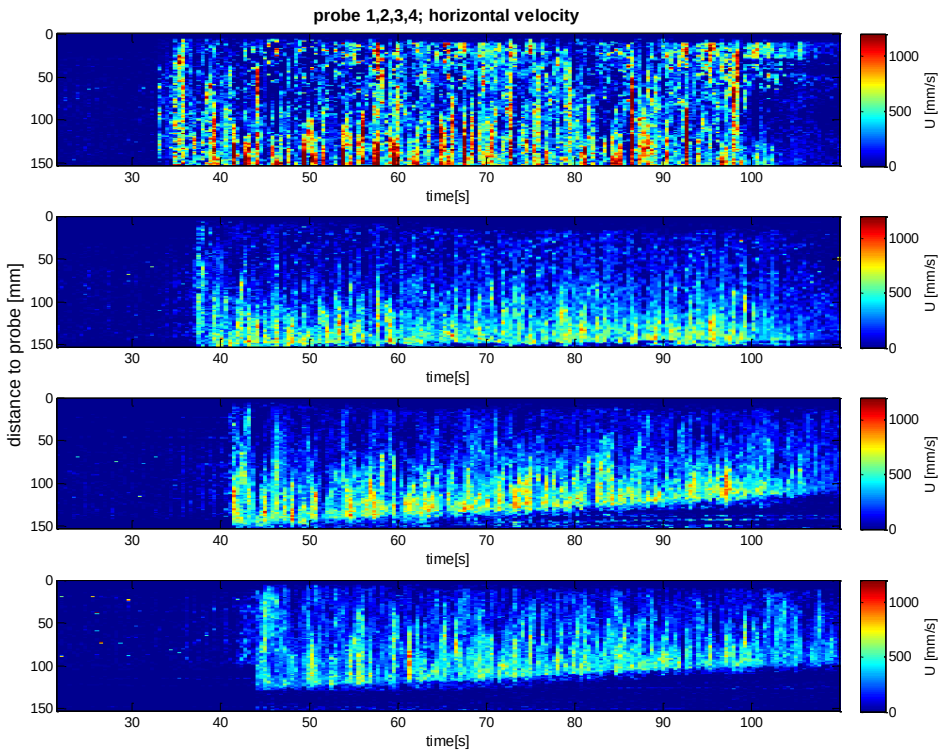

Figure 5: Velocity profiles run 44. Probe locations are indicated on the DEM (fig. 4)

For this run the first set-up for the UVP probes has been used as discussed in the methods (3D Tank), their positions have been marked on the DEM of run 44 (fig. 4). Probe 1 shows high, fluctuating velocities related to the release of entrapped air in the flow as the current enters the tank. Probe 2 shows more constant velocities with slight deposition at the base, indicated by uplift of the velocity profile. Probe 3 shows the same trend with slightly higher velocities but a significant increase in deposition. At probe 4 velocities decrease and deposition is even higher than at probe 3. These high amounts of deposition are related to the deposition of the lobe onto the slope.

Runs 49-51

Runs 49-51 can all be considered successful runs and were executed directly after each other without re-adjusting the slope in between the experiments. This was done in an attempt to simulate channel-levee evolution over several runs. The initial parameters of these runs can be found in table 2. All elevation models have been draped with a colormask, which indicates deposition/erosion with respect to the initial slope prior to run 49.

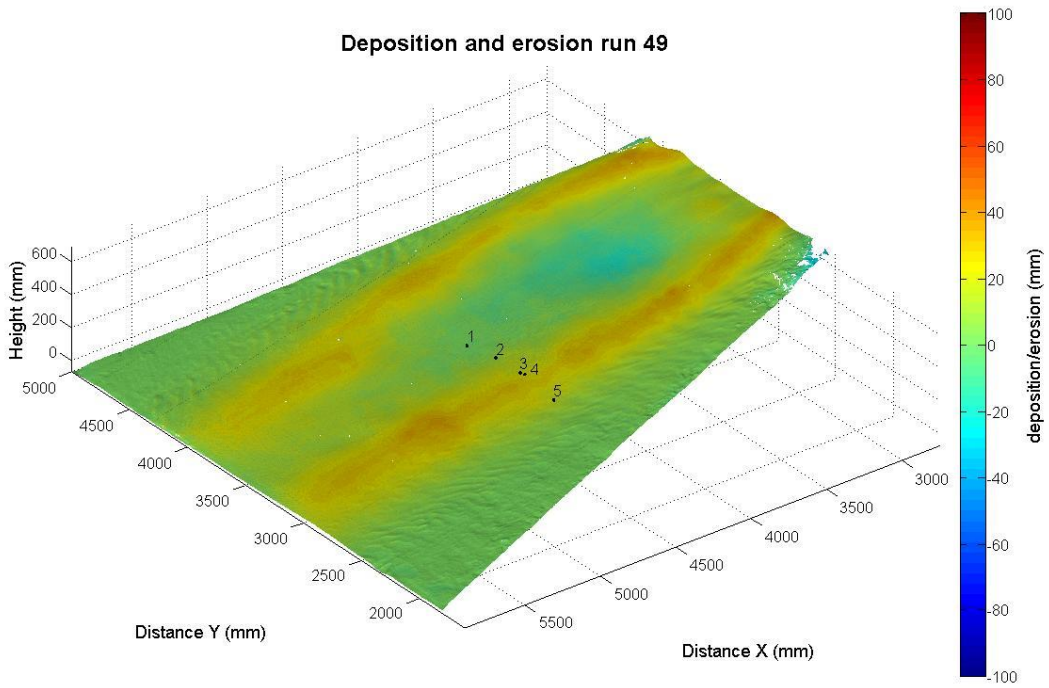

Figure 6: DEM run 49

The model (fig. 6) shows the formation of a channel bounded by levees over the entire length of the slope. The channel/levee system can be divided into 2 parts, a symmetrical lower part from x ≈ 5000 to x ≈ 6000 and a slight asymmetrical upper part from the top of the slope to x ≈ 5000. Striking in the lower symmetrical part is the deposition of sediment in the channel. This feature is shown more clearly in the cross-sections, which will be discussed later on.

Figure 7 shows the velocity data obtained by the UVP probes (1,2,4,5) of run 49. Velocity data obtained by probe 3 for all runs will be discussed later on.

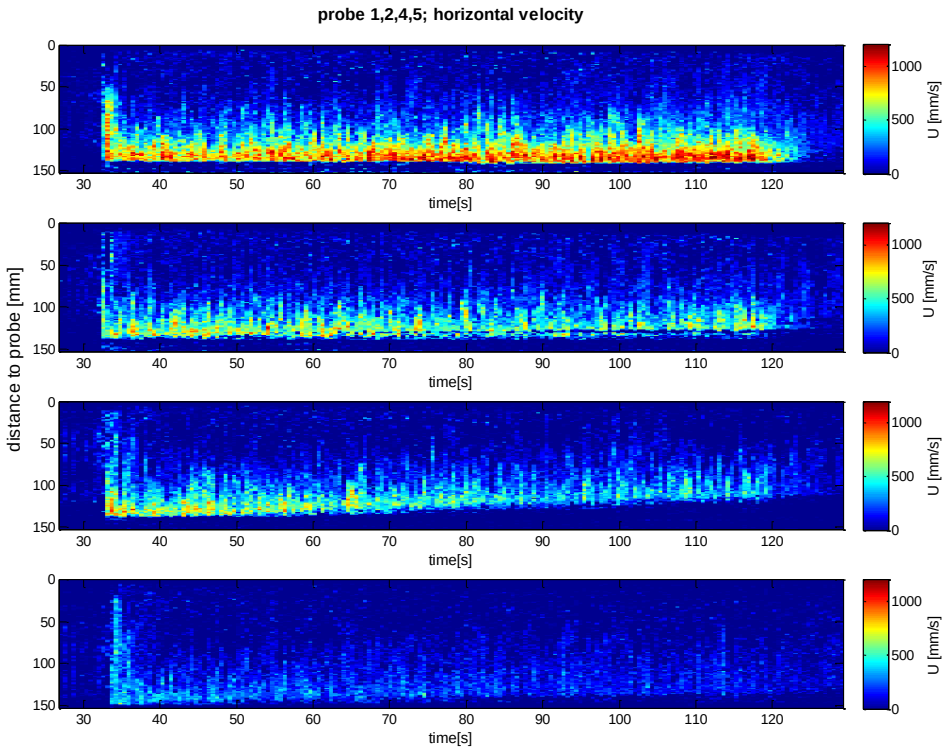

Figure 7: Velocity profiles run 49. Probe locations are indicated on the DEM (fig. 6)

For this run the second set-up for the UVP probes has been used as discussed in the methods (3D Tank). Probe 1 (placed above the left levee) shows a steady velocity profile with some minor deposition starting at x = 80 seconds till the end of the run. Probe 2 (placed above the channel) shows a velocity profile which increases during the run. Probe 4 (placed above the right levee) shows a similar pattern as at probe 1, except there is significantly more deposition and deposition starts at x = 60 seconds. At probe 5 (placed at the right side of the right levee) almost no flow occurs except in the first 5 seconds of the run. Another interesting observation is the decrease in velocity at probe 5, and the increase in velocity at probe 1 when levee formation starts. The formation of levees starts at x = 60 seconds, which is visible in the profile of probe 4.

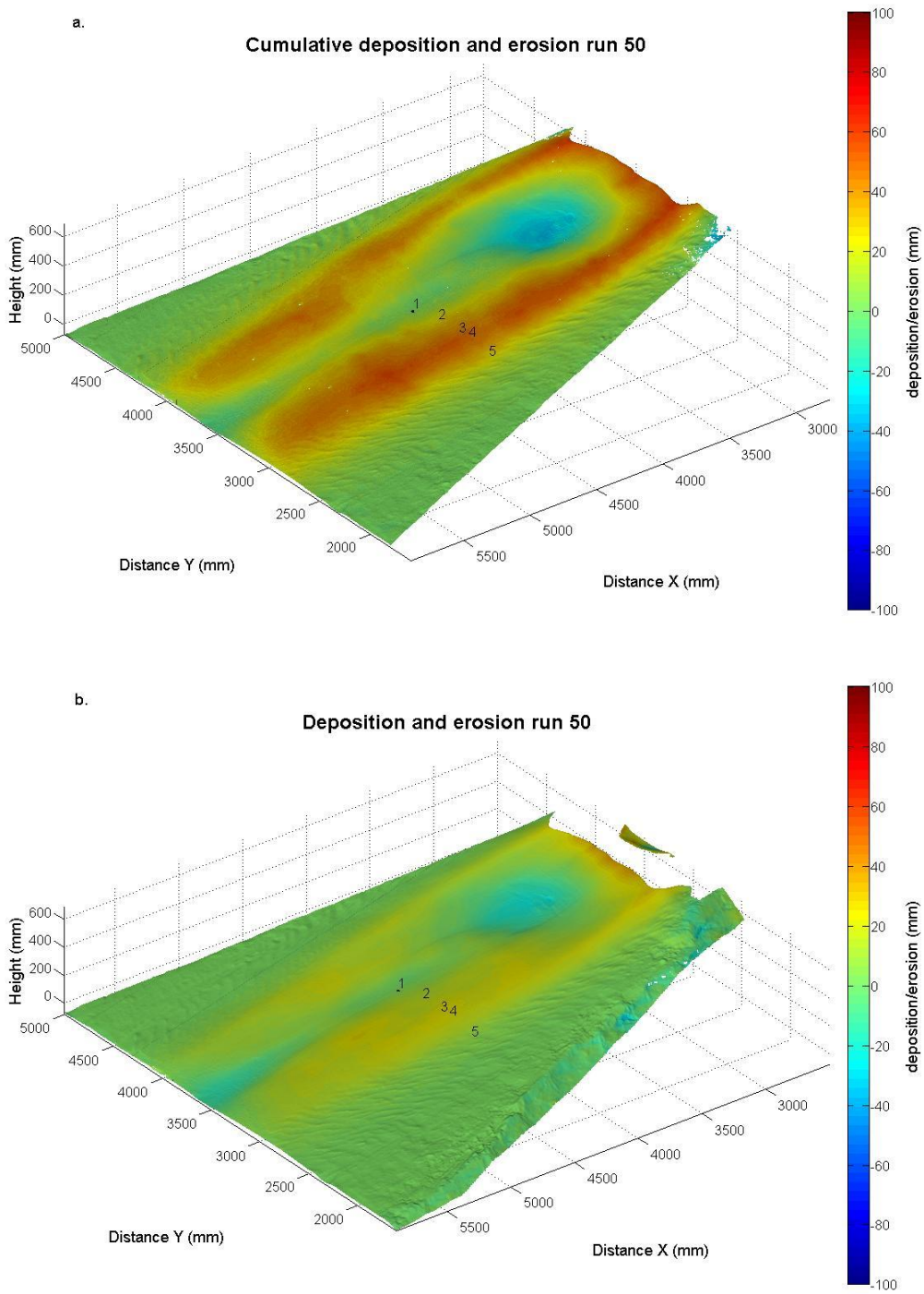

Figure 8: (a) Cumulative DEM of run 50 including the deposition and erosion of run 49. (b) DEM run 50.

Run 50 was executed directly after run 49. The white spot in fig. 8a,b at the upper part of the slope indicates the position of the inlet box. The model shows further development of the channel/levee system on the slope as well as the scour. The symmetrical lower part has increased to x ≈ 4000, and the levees in the lower part have significantly increased in width and height. The upper part is still

asymmetrical which is probably caused by the scour. The levees in the asymmetrical part have increased in height but not so much in width. The scour in front of the inlet box has not increased much in size, but has eroded further into the slope. Fig. 7b clearly shows the development of the levees, increasing erosion at the scour and incision in the channel at the lower part of the slope.

Figure 9 shows the velocity data obtained by the UVP probes of run 50.

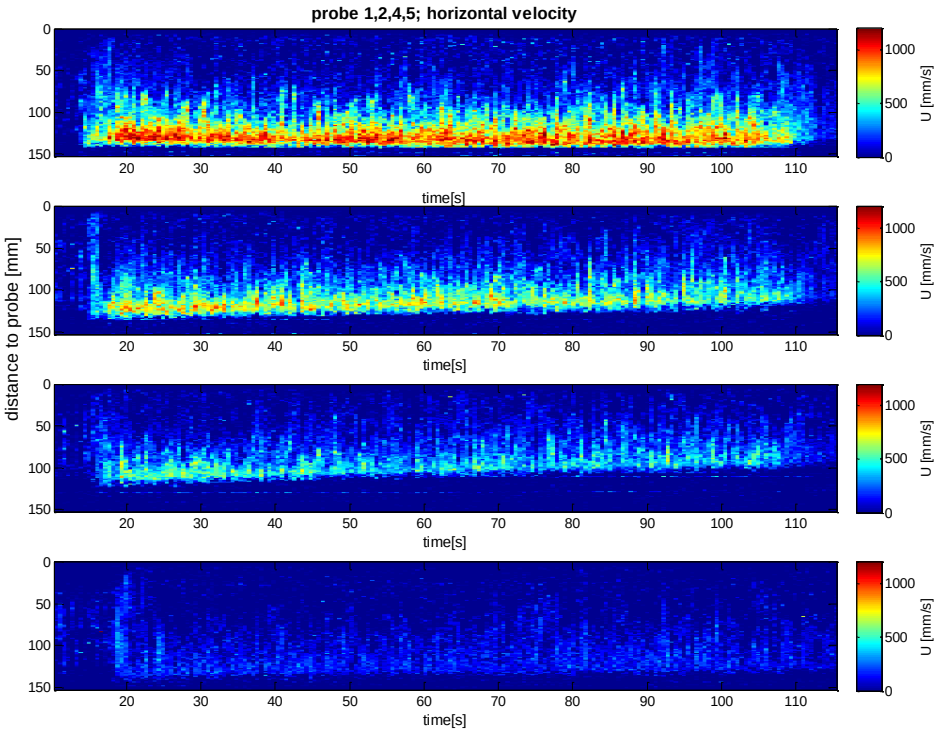

Figure 9: Velocity profiles run 50. Probe locations are indicated on the DEM (fig. 8)

For this run the second set-up for the UVP probes has been used as discussed in the methods (3D Tank). All of the velocity profiles show a very similar pattern as the velocity profiles of the previous run (run 49). The velocity at probe 1 remains more or less unaltered compared to the velocity at run 49, deposition continues during this run. Velocities at probe 2, located above the channel, have increased. The velocity at probe 4 has decreased while deposition continues during the run at the same rate. The velocity at probe 5 has also decreased with respect to the previous run.

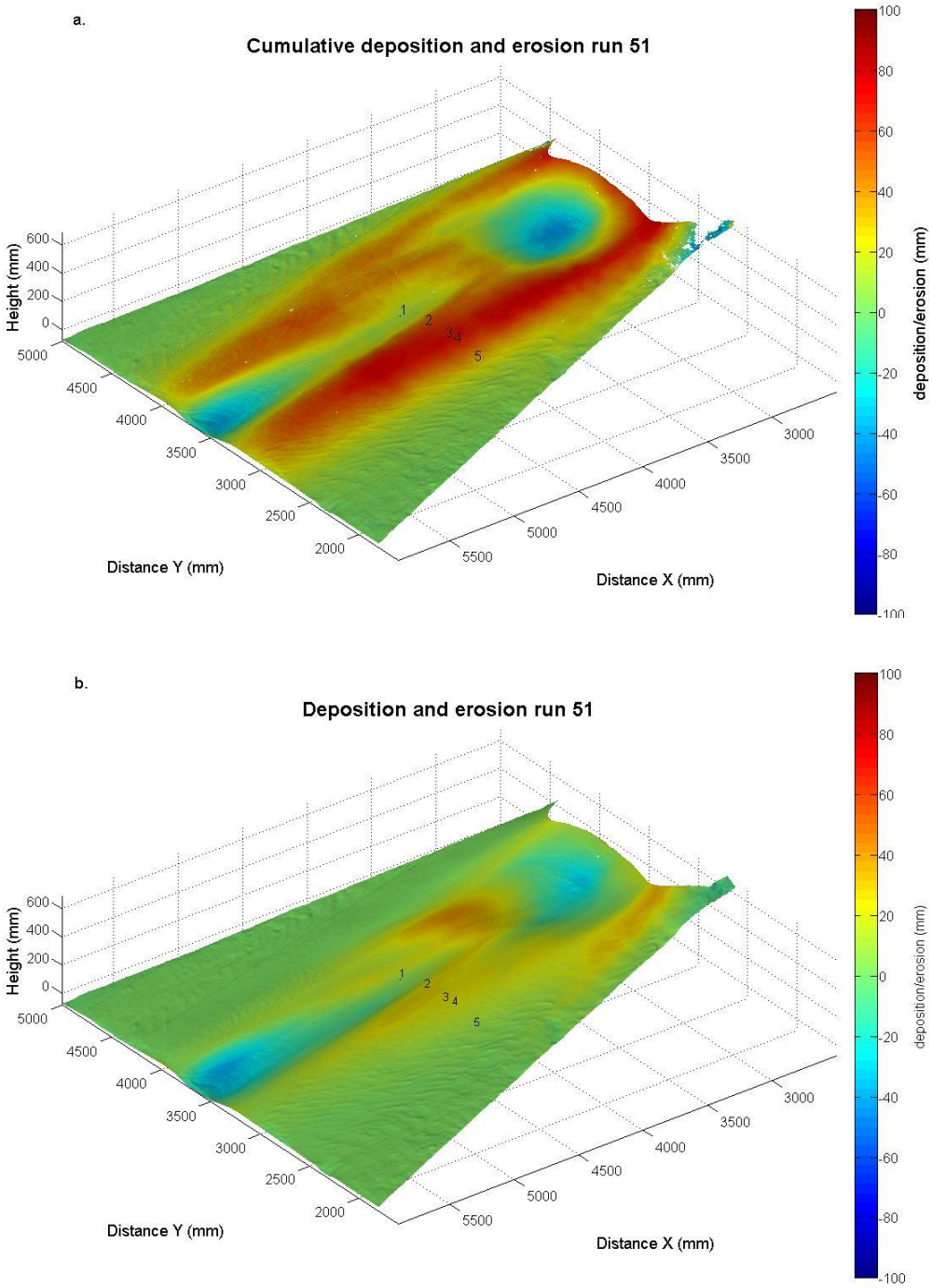

Figure 10: (a) Cumulative DEM of run 51 including the deposition and erosion of run 49 and run 50. (b) DEM run 51.

Run 51 was executed directly after run 50. The white spot in fig. 10a,b at the upper part of the slope indicates the position of the inlet box. The symmetrical lower part now reaches to x ≈ 3750 and the height of the levees have increased, especially the right levee. Incision of the channel into the slope has increased at the lower part of the slope. The upper part became less asymmetrical due to the development of the levees but it is still present due the existence of the scour, which again has eroded further into the slope. Remarkably, the levee on the right has developed more than the levee

on the left. Fig. 10b shows extensive incision in the lower part of the slope and increased erosion in the scour. Levee development is prominent in the upper part of the slope and decreases in both height and width down slope.

Figure 11 shows the velocity data obtained by the UVP probes of run 51.

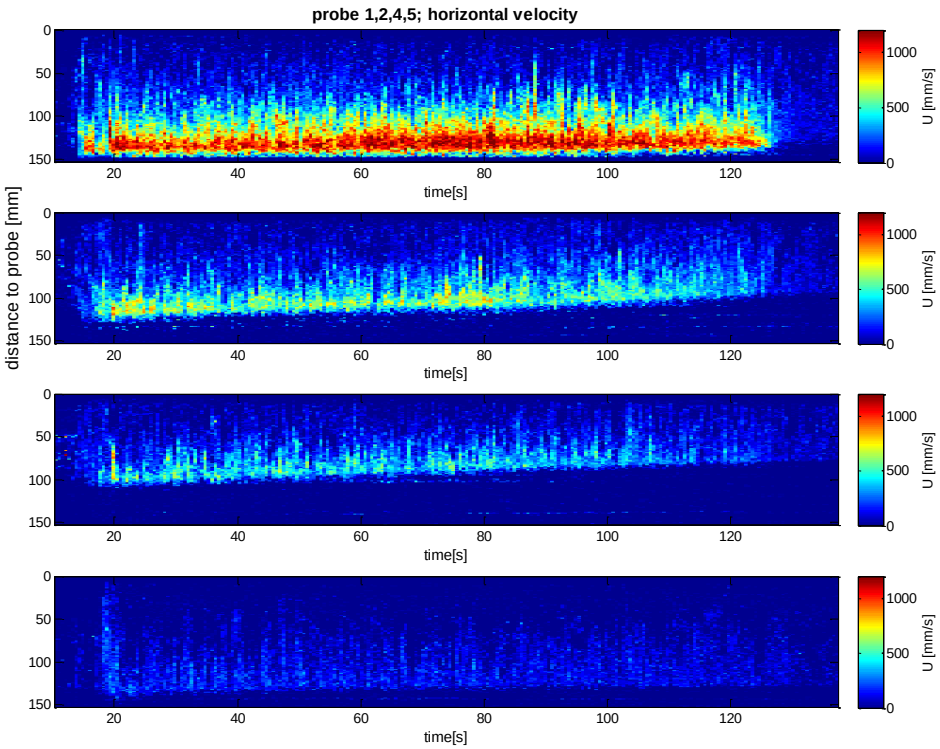

Figure 11: Velocity profiles run 51. Probe locations are indicated on the DEM (fig. 10)

Again the profiles show a similar pattern as in the previous runs (runs 49 and 50). Deposition continues at probe 1 while the velocity remains constant. The velocity in the channel at probe 2 has increased significantly. Velocities at probe 5 remain close to zero.

Figure 12 shows the velocity data obtained by probe 3 for all runs (49-51). Note that the colours of the colour bar are inverted, this was done in order to get a clear velocity profile.

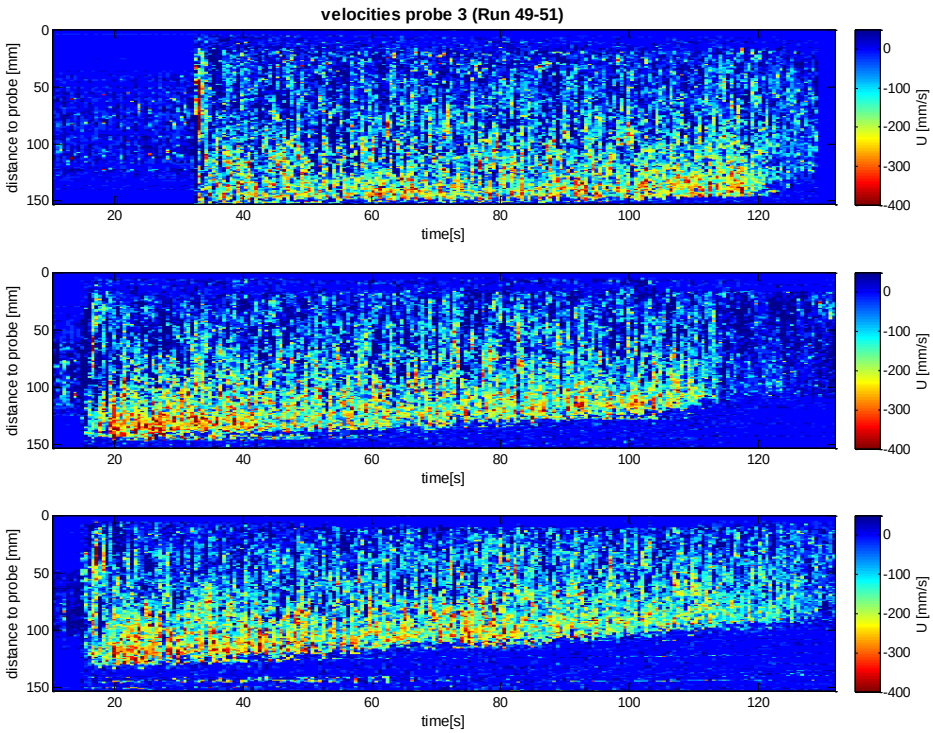

Figure 12: Velocity profiles of probe 3 for all runs. Position of probe 3 is inidicated on the DEM's (fig. 6, 8 and 10)

Probe 3 was oriented along-strike to measure the velocity of flow along the strike of the slope. Blue colours indicate flow towards the edge of the slope, while the red colours indicate flow towards the centre of the slope. A trend seems to be visible in the velocity profiles (fig. 12) in which the profiles can be divided into 2 parts, an upper part and a lower part. The upper part is dominated by blue colours, while the lower part is dominated by red colours. This phenomenom is however not very distincitive and is more strongly present in the first 40 seconds of the velocity profiles, especially in the profiles of runs 50 and 51.

Also noticable in the velocity profiles is the amount of deposition at the location of the probe. In the first run almost no deposition occurs untill the end of the run. Deposition increases in runs 50 and 51 which can be related to the extension of the levees. Due to the formation of levees the bedding plane rises and the distance to the probe decreases (visible in runs 50 and 51 in figure 12).

In all the runs the velocity profiles obtained at probe 3 show very similar patterns, with an upper part dominated by dark-red colours and a lower part dominated by blue colours. Which indicated flow to the edge of the slope and flow towards the centre of the slope (towards the channel). This pattern will be analyzed in detail in the discussion section of this report.

Cross-sections

Further data analysis in this study will concentrate on the data obtained in runs 49-51. These runs are most successful and present outstanding experimental data on the evolution of a turbidite channel and its levees. Cross-sections have been made from X = 4100 to X = 5800 from which data is obtained concerning the evolution of a turbidite. This interval has been chosen because the evolution of the channel and levees remain stable throughout the experiments, and is therefore suitable for evaluation. Four cross-sections which were made at X = 4100, 4470 (at the probes position), 5000, 5700 (fig. 13) are shown for a quick evaluation.

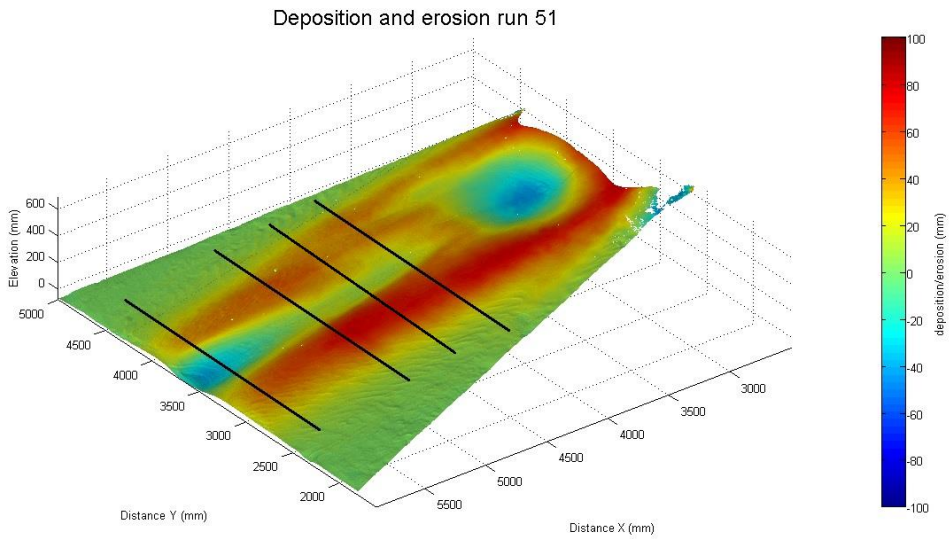

Figure 13: Location of given cross-sections at X = 4100 (fig. 13), 4470 (fig. 14), 5000 (fig. 15) and 5700 (fig. 16).

Figure 14 shows the cross-section at x = 4100.

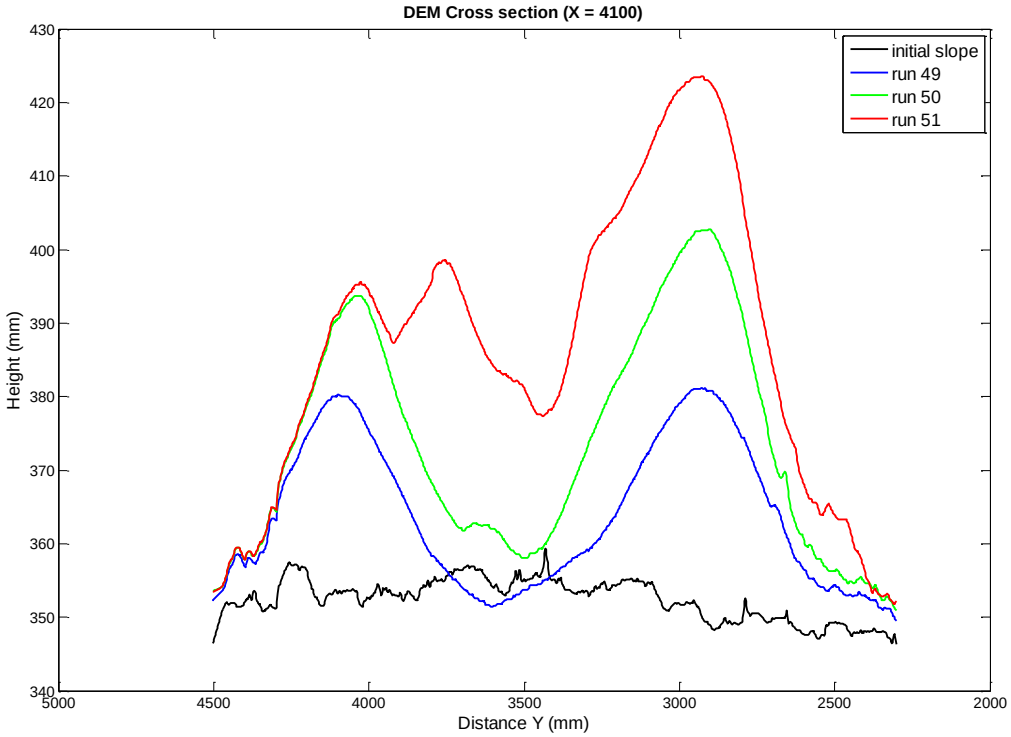

Figure 14: Cross-section runs 49-51 (at X = 4100)

The cross-section shows the formation of channel and levees in run 49 and further development in runs 50 and 51. The right levee (levee 1) shows a more or less steady evolution in which the thickness of the levee is already set in the first run and the levee only increases in height in the following runs. The left levee (levee 2) shows the same process for runs 49 and 50 but undergoes an abrupt change in run 51. The original levee is abandoned and a new levee is formed closer to levee 1, narrowing the channel. The channel is slightly erosional in run 49 but shifts towards a depositional channel in runs 50 and 51. The channel is narrowed in run 51 and the channel thalweg is located near levee 1.

Figure 15 shows the cross-section at x = 4470

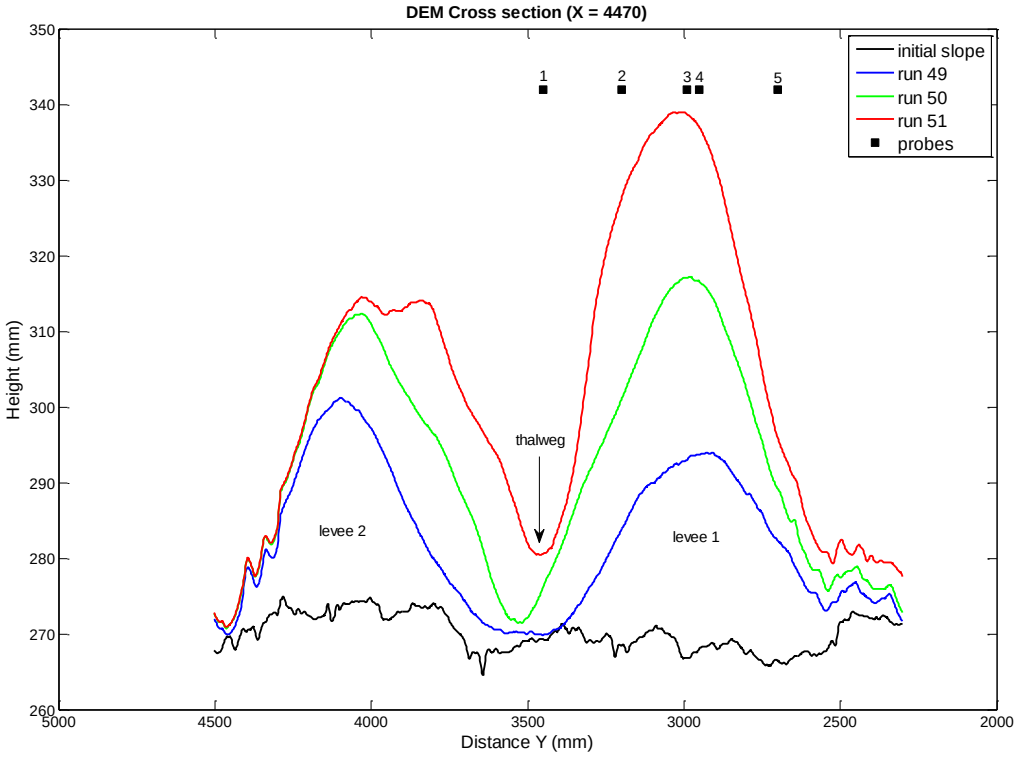

Figure 15: Cross-section runs 49-51 (at X = 4470) with position of the probes and annotation (right levee is levee 1, left levee is levee 2).

This cross-section shows a very similar pattern as the previous cross-section (fig. 14). The evolution of levee 1 is the same. Also visible is the gradual shifting of levee 1 towards the centre, this is best noticeable by looking at the crest of levee 1 which shifts towards the centre in time. This process is decreasing the channel width after each consecutive run. The evolution of levee 2 is also very similar with a shift towards the channel in run 51, however the levee is not separated into two parts but remains one entity. The development of levee 2 is significantly lower than the development of levee 2 during run 51. Deposition in the channel occurs in all runs and the channel thalweg shifts towards levee 1 during each run.

Figure 16 shows the cross-section at x = 5000

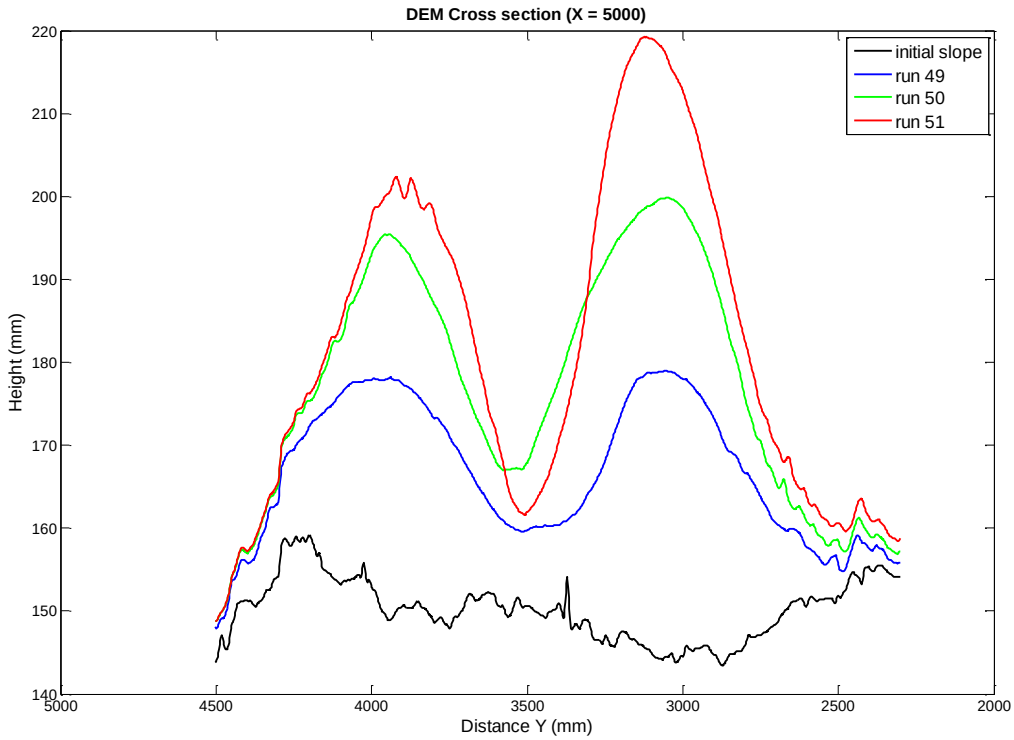

Figure 16: Cross-section runs 49-51 (at X = 5000)

This cross-section at X = 5000 shows some minor differences compared to the previous cross-sections. Levee 2 remains intact in all of the experiments, the irregular shape on top of levee 2 can be associated with the formation of ripples by the turbidity current spilling over the levee. Also the channel thalweg remains more in the centre of the channel. The most striking difference is the incision of the channel into the previous deposits in run 51, meaning that the turbidity current is no longer depositional in the channel.

Figure 17 shows the cross-section at x = 5700

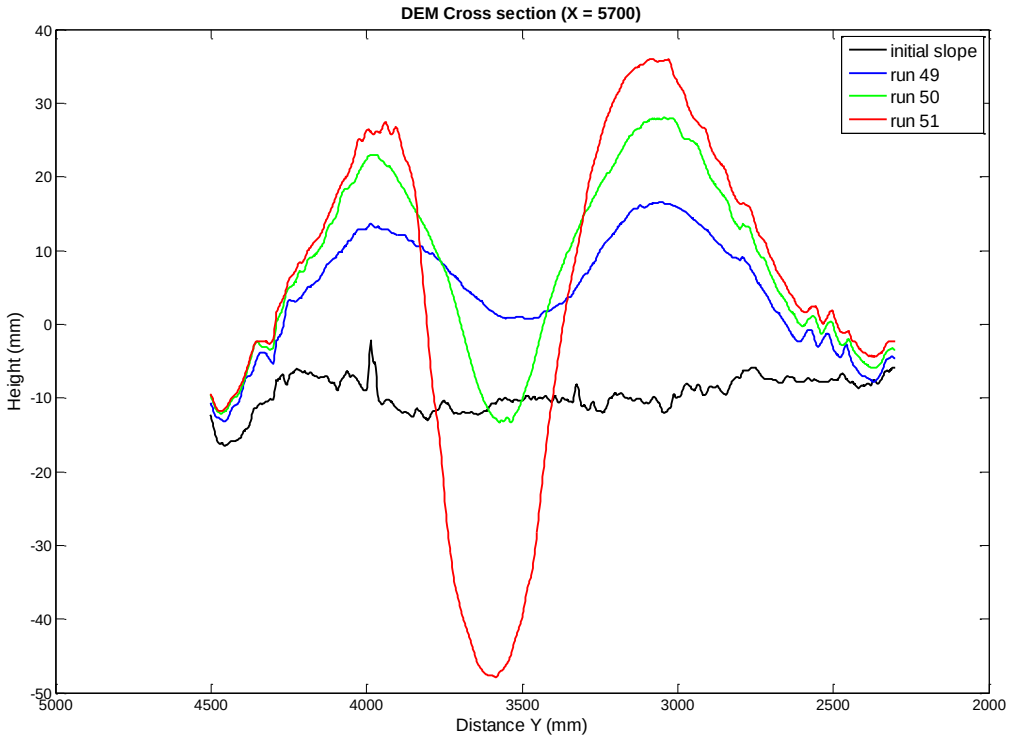

Figure 17: Cross-section runs 49-51 (at X = 5700)

Incision of the channel into previous deposits starts during run 50. The rate of incision is higher than in the cross-sections at x = 4100, 4470, 5000 (fig. 14-16). Channel incision in run 51 excises to a level well below that of the initial slope. This increasing incision is associated with an increase of the depth/width ratio of the system (see also fig. 29 & 30).

Data analysis

Data analysis will be performed from x = 4100 down slope to x = 5800 (see fig. 9a), this is done in order to avoid the area affected by the scour which could have a significant effect on the process of channel and levee formation. All the definitions of the metrics used in the data analysis are illustrated in figure 18.

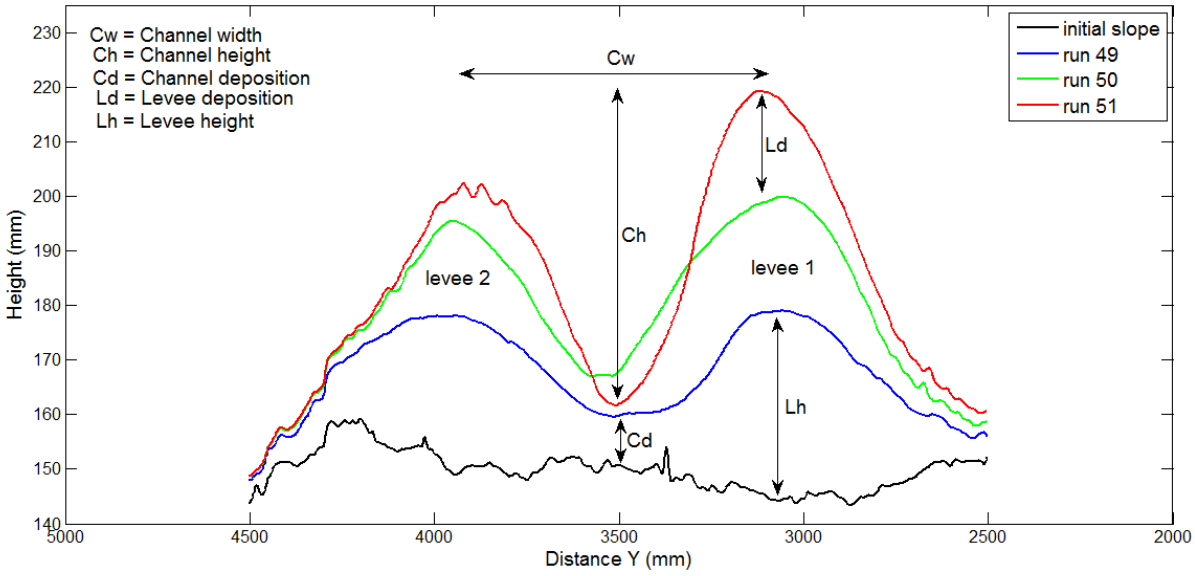

Figure 18: Metrics used in the data analysis section. Channel width (Cw) is defined as the distance between the levee crests. Channel height (Ch) is defined as the distance between the deepest point of the channel and the heighest levee crest. Channel deposition (Cd) is defined as the amount of deposition between the deepest point of the channel and the initial slope. Levee deposition (Ld) is defined as the amount of deposition between levee crests of each run. Levee height (Lh) is defined as the distance between levee crest and the initial slope.

The cross-sections show that the entire system starts in a depositional state in run 49 (from x = 4100 down slope), in which the amount of deposition in the channel increases down slope (with increasing X), while the amount of deposition at the levees remains more or less constant (fig. 19a,b,c). In the consecutive runs the system gradually changes to a erosional state in the channel, in which the rate of incision in the channel increases down slope (fig. 19a). Deposition continues on both levees, the amount of deposition however decreases down slope (fig. 19a,b). Levee 2 even shows some phases of slight erosion (fig. 19c). Deposition in the channel has been measured at the deepest point of the channel. Deposition on the levees has been measured at the levee crests (see fig. 18).

This raises the question which process causes this change in state. A change from deposition to erosion has to be caused by a change in the erosive force of the current. This force is mainly determined by the kinematic energy of the current. Therefore a change from deposition to erosion is

most likely caused by changes in kinematic energy (i.e. velocity). There are several ways to increase the kinematic energy of a turbidity current; An increase in input velocity, confinement of the current by the build-up of levees or an increase in the slope gradient. Since the input parameters were kept constant during this study the first option can be neglected. This leaves the options of confinement of the flow or an increase in gradient.

Figure 20a,b,c and figure 21a,b,c,d show the time-averaged velocity profiles of probes 1,2,4 and 5 of all the runs (location of the probes can be found in fig. 15). Figure 20 shows the profiles per run, figure 21 shows the profiles per probe. Time-averaged profiles have been taken from the body of the turbidity current of each run; run 49 from 35-115 s, run 50 from 25-105 s, run 51 from 30-120 s (see fig. 7,9 and 11).

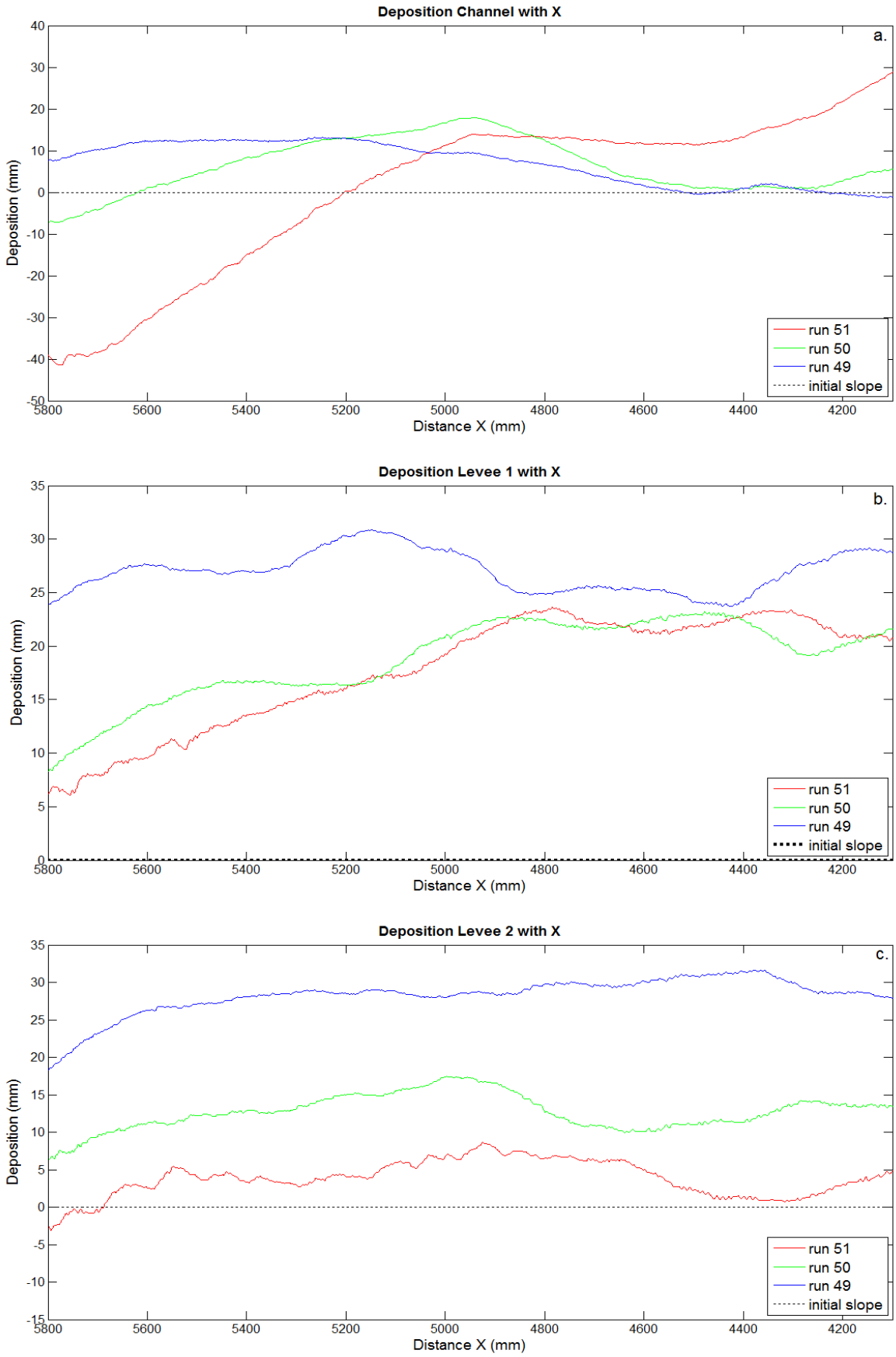

Figure 19: (a) Channel deposition/erosion measured between the deepest point of the channel and the initital slope (see fig. 18). Deposition occurs over the entire length of the channel during run 49. In runs 50 and 51 deposition continues at the upper part of the slope (from x = 4100 – 4800) while erosion increases significantly at the lower part of the slope (from x = 4800 – 5800). (b) Levee 1 deposition measured between the levee crests of each run (see fig. 18). (c) Levee 2 deposition measured between the levee crests of each run.

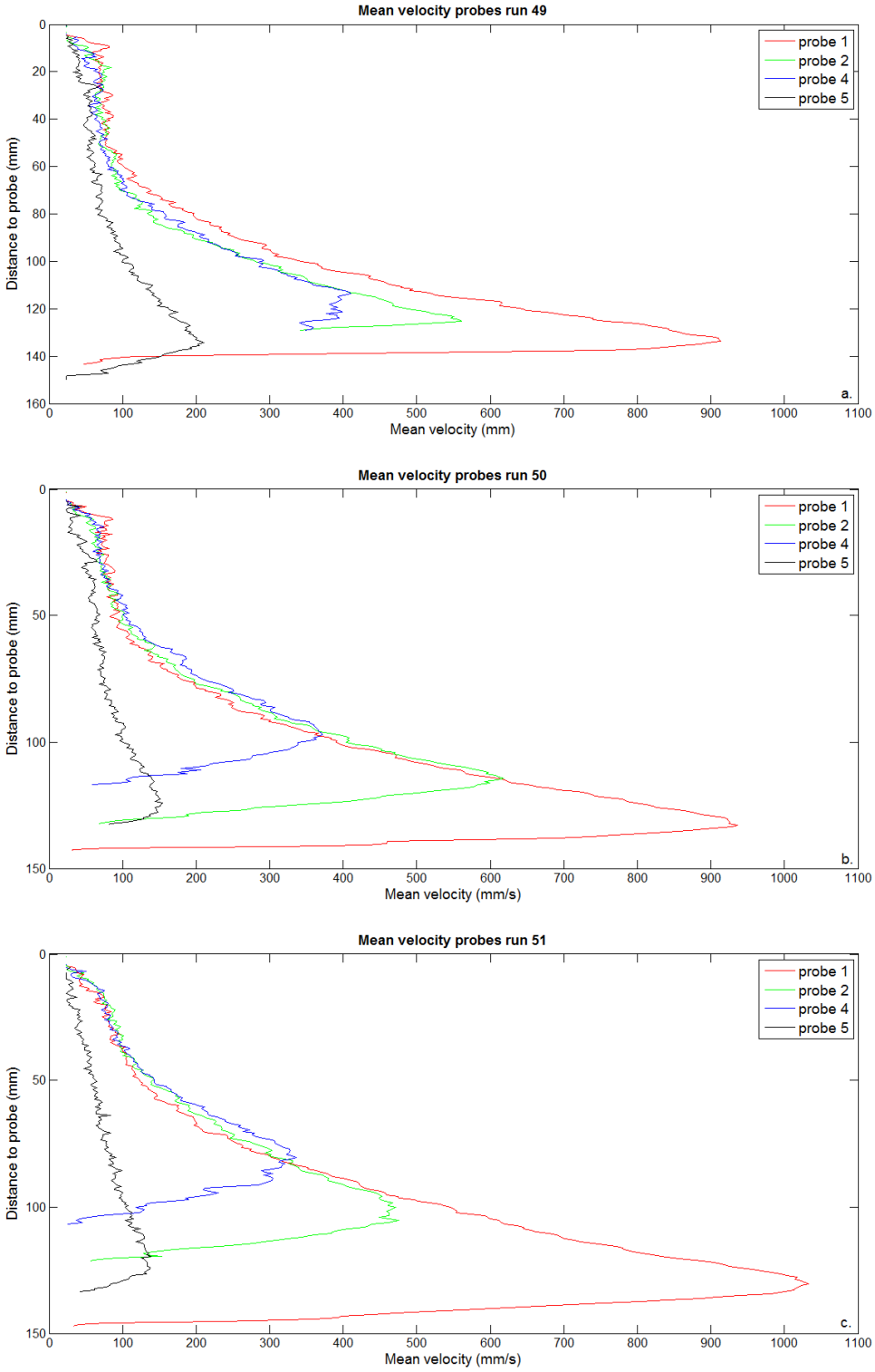

Figure 20: Time-averaged velocities (mm/s) of probes 1,2,4 and 5 of runs 49-51. (a) Mean velocity run 49. (b) Mean velocity run 50. (c) Mean velocity run 51. Probes 1,2,4 and 5 are placed along the strike of the slope, from the channel-axis to outside the levee (see also fig.15).The velocity profiles show the decrease in velocity from the channel towards outside the levees.

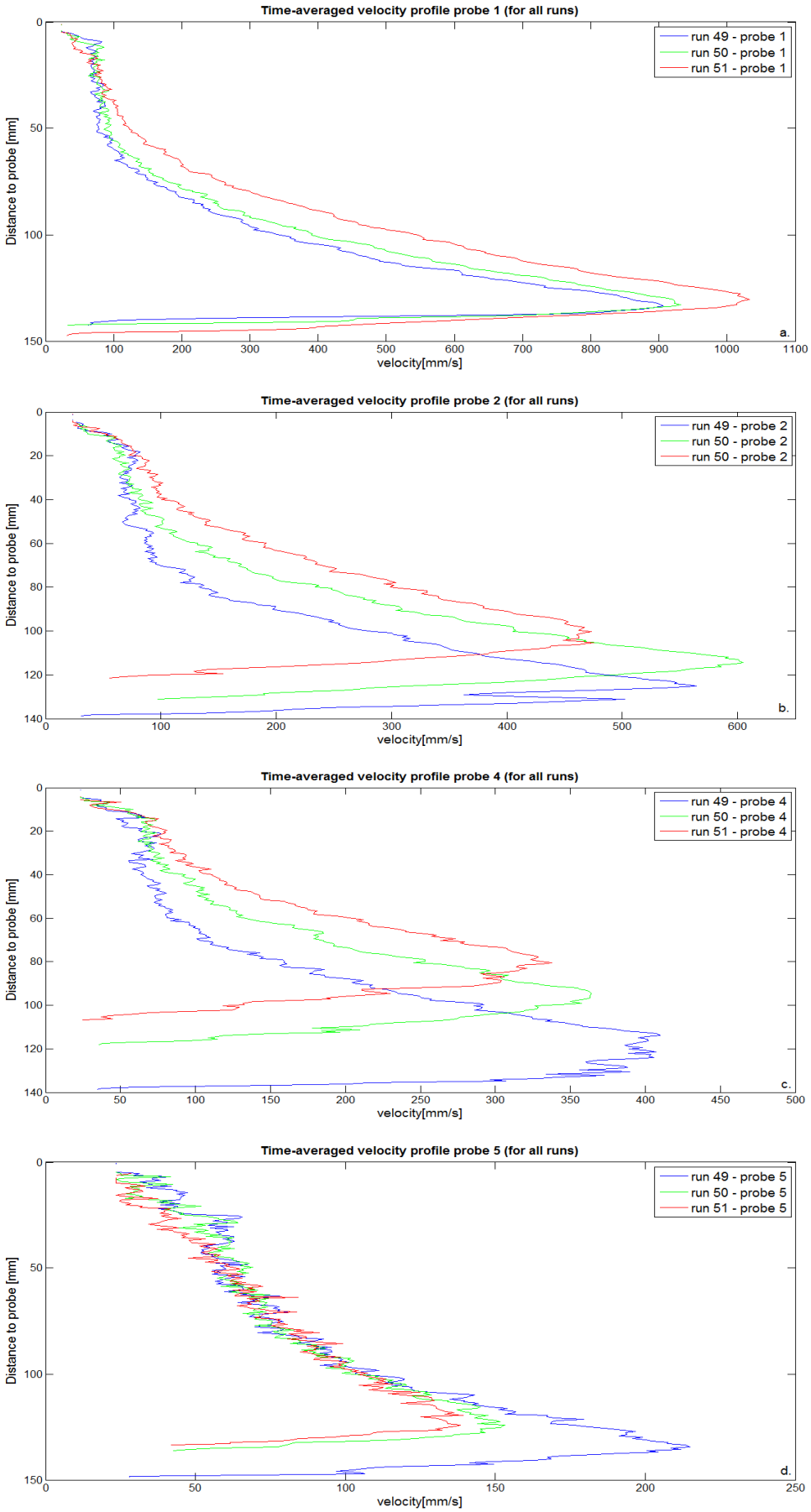

Figure 21: Time-averaged velocity profiles (mm/s) of probes 1,2,4 and 5 of runs 49-51. (a) Time-averaged velocity of probe 1 (runs 49-51) positioned in the channel. (b) Time-averaged velocity of probe 2 (runs 49-51) positioned between channel and the crest of levee 1. (c) Time-averaged velocity of probe 4 (runs 49-51) positioned at the crest of levee 1. (d) Time-averaged velocity of probe 5 (runs 49-51) positioned outside levee 1. The profiles show increasing velocities at probe 1 and decreasing velocities at probes 2,4 and 5.

Figure 20 shows a decrease in velocity from the channel towards outside the levee along the strike of the slope. Channel velocities are significantly higher than the velocities measured at levee 1 and outside levee 1. Figure 21 shows and evident trend of decreasing velocities in each consecutive run at probes 2,4 and 5 while velocities at probe 1 are increasing. This increase in velocity in the channel (probe 1) and the (slight) decrease in velocity on top of levee 1 (probe 4) and outside levee 1 (probe 5) is also well shown in figure 22a,b,c. Also illustrated in figure 22 is the decrease in velocity of the turbidity current along the strike of the slope (from channel to levee 1 to outside levee 1), and the corresponding changes in channel-levee morphology throughout the experiments.

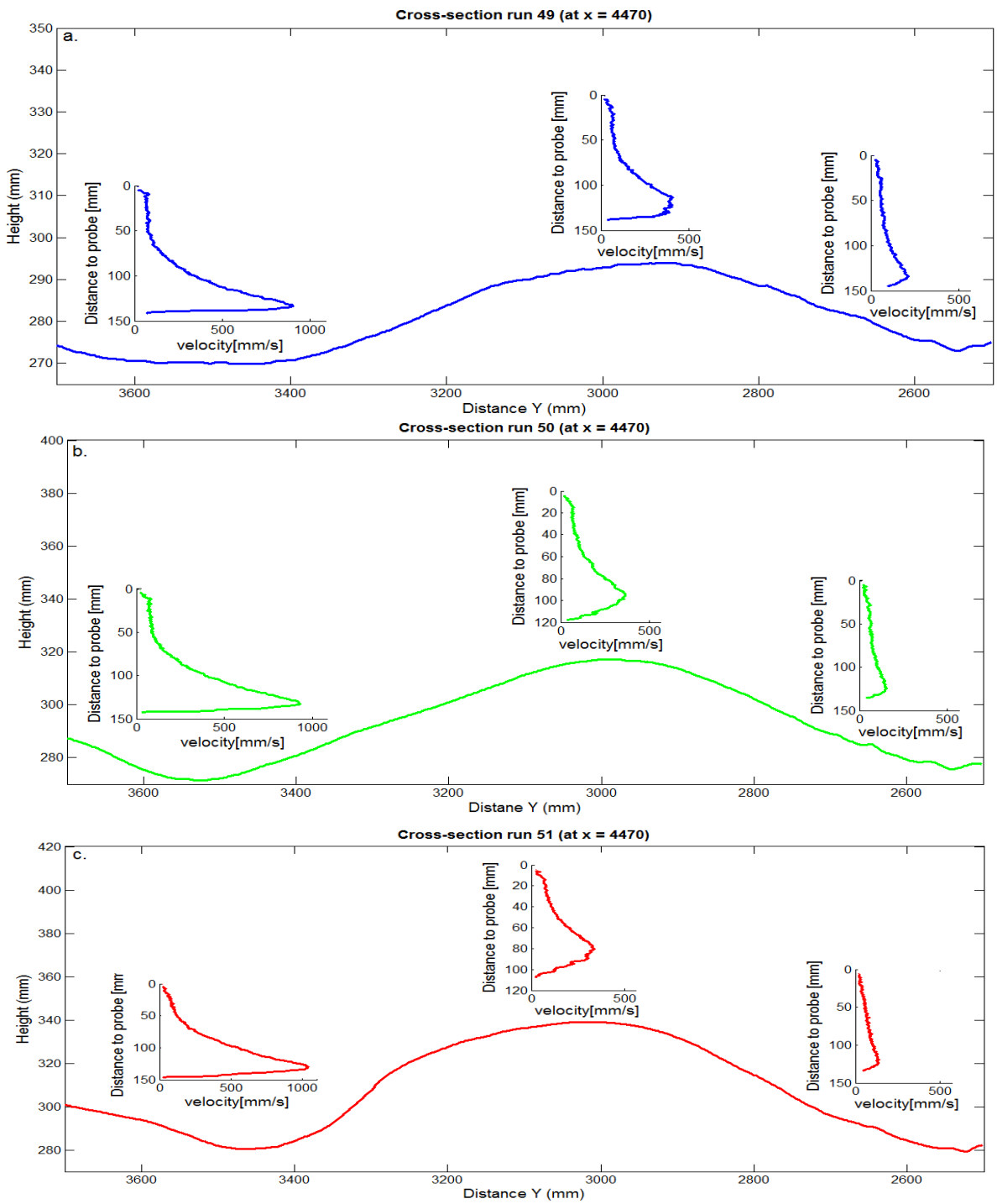

Figure 22: Time-averaged velocities (mm/s) plotted with channel and levee (1) morphology. (a) Time-averaged velocity probe 1,4 and 4 run 49. (b) Time-averaged velocity probe 1,4 and 5 run 50. (c) Time-averaged velocity probe 1,4 and 5 run 51.Left profile is probe 1 (channel velocity), middle profile is probe 4 (levee velocity), right profile is probe 5 (outside levee).

Figure 23 shows the gradient in the channel after each run, which is one of the possible parameters responsible for the increase in channel velocity.

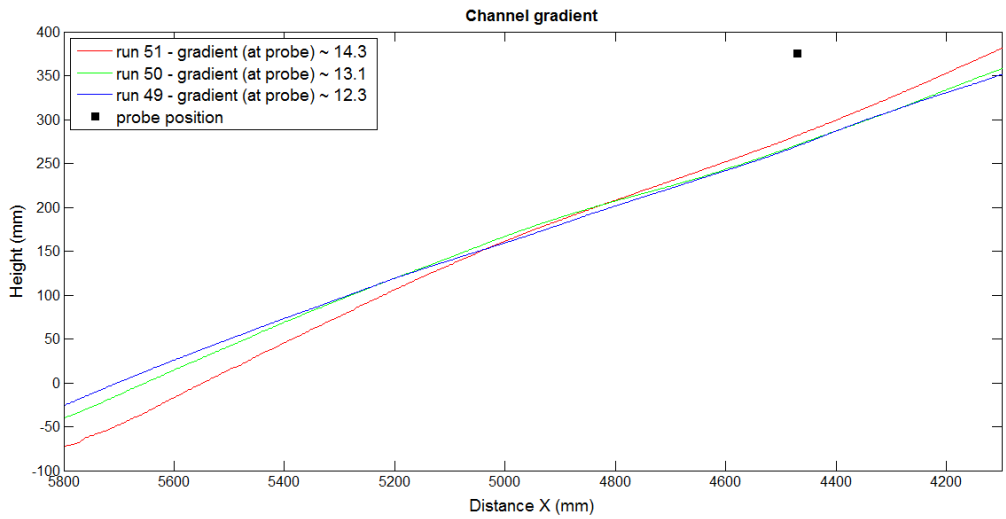

Figure 23: Evolution of the channel gradient over the entire analyzed slope (from x = 4100 – 5800). The gradient at the probe has been measured over distance x = 4100 - 4600.The figure shows an increase of the channel gradient over time.

Figure 23 shows an increase of the channel gradient at the position of the probe where the velocity profiles were obtained from run 49 to run 51. The channel gradient in run 49 is ~12.3°, in run 50 it is ~13.1° and in run 51 it is ~14.3°. The gradient has been calculated over the interval X = 4100 – 4600.

The velocity measured at the crest of levee 1 (probe 4) slightly decreases (fig. 21c). This could be caused by a slight decrease in the gradient at the position of probe 4. Figure 24 shows the gradient at probe 4.

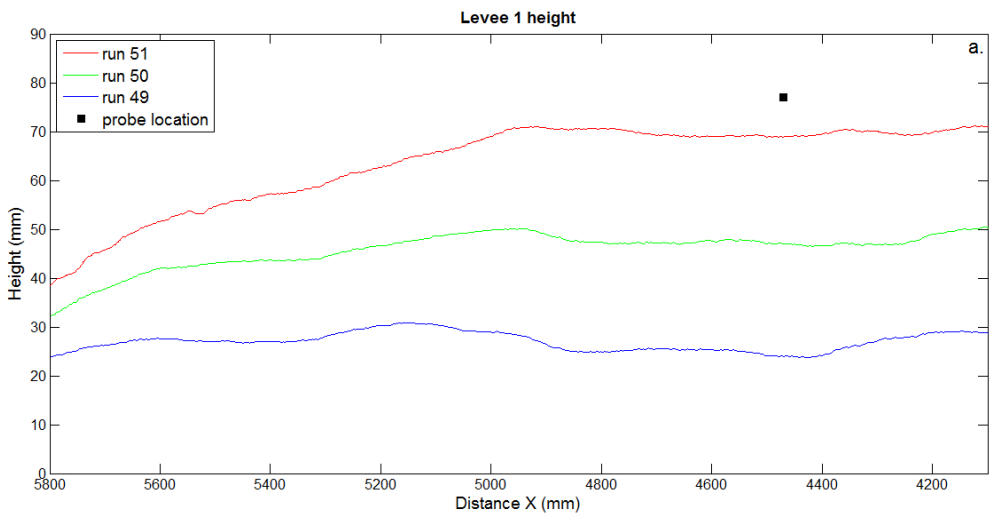

Figure 24: Height of levee 1 measured from levee crest to initial slope (see fig. 18). The profiles also illustrate the gradient of levee 1 from x = 4100 – 5800.

Figure 24 shows no significant changes in gradient at the probe position. There is however a decrease of the gradient upstream of the probe (from X = 4100 – 4400) which could cause a slight decrease in velocity measured at the probe.

Another mechanism which can lead to increasing velocities in the channel is confinement of the flow, focusing the turbidity current through the channel. This process gains more influence when the channel depth increases and levee height increases. Figure 25a,b,c,d shows the channel depth, channel width and the height of levees 1 and 2 along the slope.

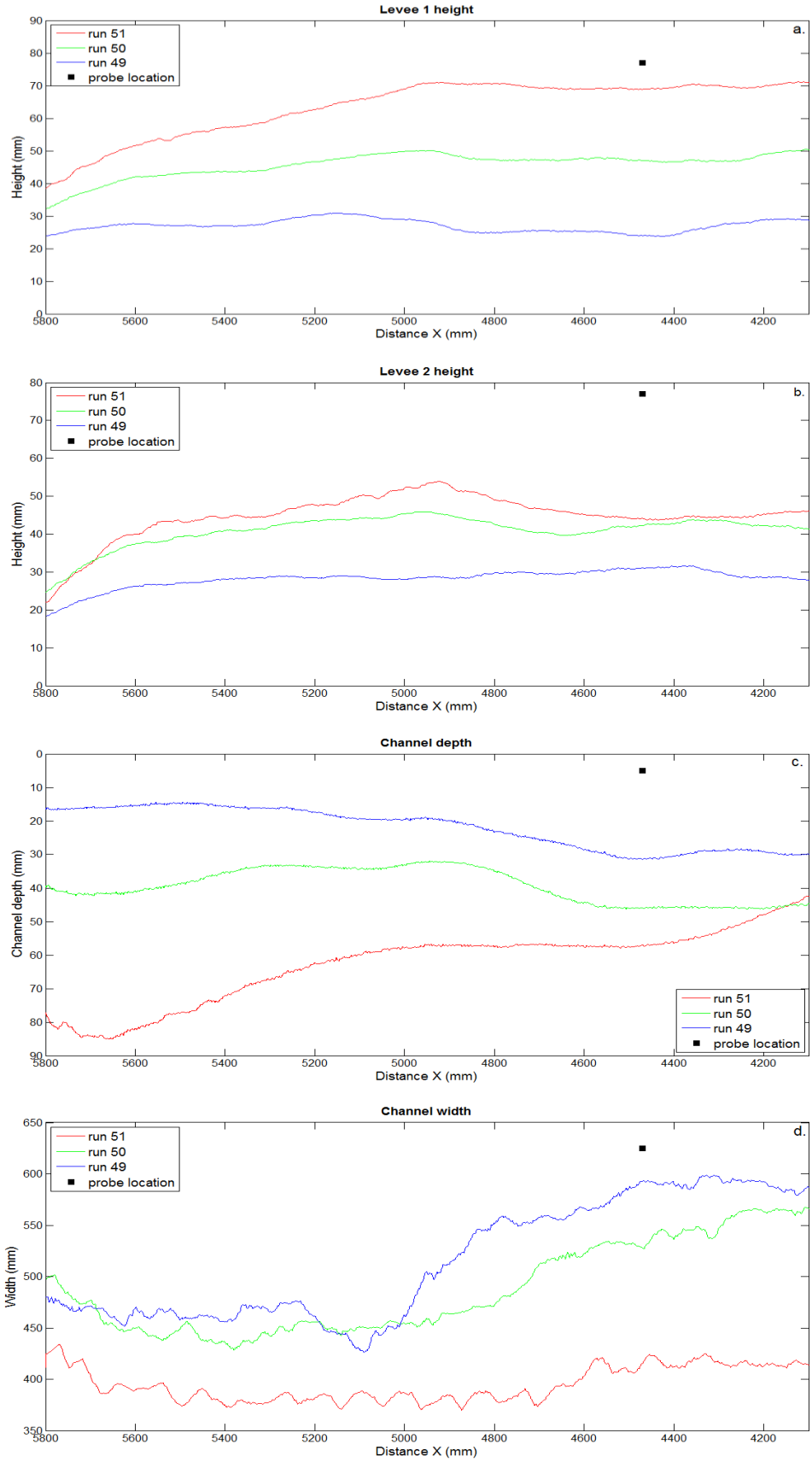

Figure 25: (a) Levee 1 heigth (mm), measured from the initial slope to levee crest (see fig. 17). (b) Levee 2 heigth (mm), measured from the initial slope to levee crest (see fig. 18). (c) Channel depth (mm), measured from levee crest to the deepest point in the channel (see fig. 18). (d) Channel width (mm), measured from levee crest to levee crest (see fig. 18).

The channel depth (fig. 25c) at the location of the probes (X = 4470) increases from 32 mm (run 49) to 46 mm (run 50) to 57 mm (run 51). The height of levee 1 is considerably larger than the height of levee 2 (fig. 25a,b). The height of levee 1 increases from 24 mm (run 49) to 47 mm (run 50) to 69 mm (run 51) while the height of levee 2 only increases from 31 mm (run 49) to 42 mm (run 50) to 44 mm (run 51). Striking is the minimal increase (2 mm) from run 50 to run 51 which is also the moment in which levee 2 shifts towards the channel (fig. 15). This is also well visible in Figure 24d, which shows the channel width along the slope. The channel width has been defined as the distance between both levee crests (see fig. 18). The channel width shows no significant decrease from run 49 to run 50 but shows a large decrease from run 50 to run 51 which is mainly caused by the shift of levee 2.

Channel narrowing along with an increasing channel depth and increasing levee heights are parameters which enhance confinement of the turbidity current which can significantly enhance the velocity of the turbidity current in the channel.

Backslope

The backslope of a levee is defined as the profile from the proximal part of the levee towards the distal part of the levee. This particular subject has been analysed in great detail for its shape, and the variation in shape down slope in previous studies (e.g. Straub & Mohrig, 2008; Nakajima & Kneller, 2013; Ezz et al., 2014). The backslope of levee 1 has been analysed for its shape for runs 49-51 in steps of 250 mm from x = 4100 (upslope) to x = 5850 (downslope). Figure 25a,b,c shows the profiles of the backslope of levee 1 for run 49 (fig. 26a), run 50 (fig. 26b), and run 51 (fig. 26c). The figure shows a transition of the profile of levee 1 from upslope (x = 4100) to downslope (x = 5850).

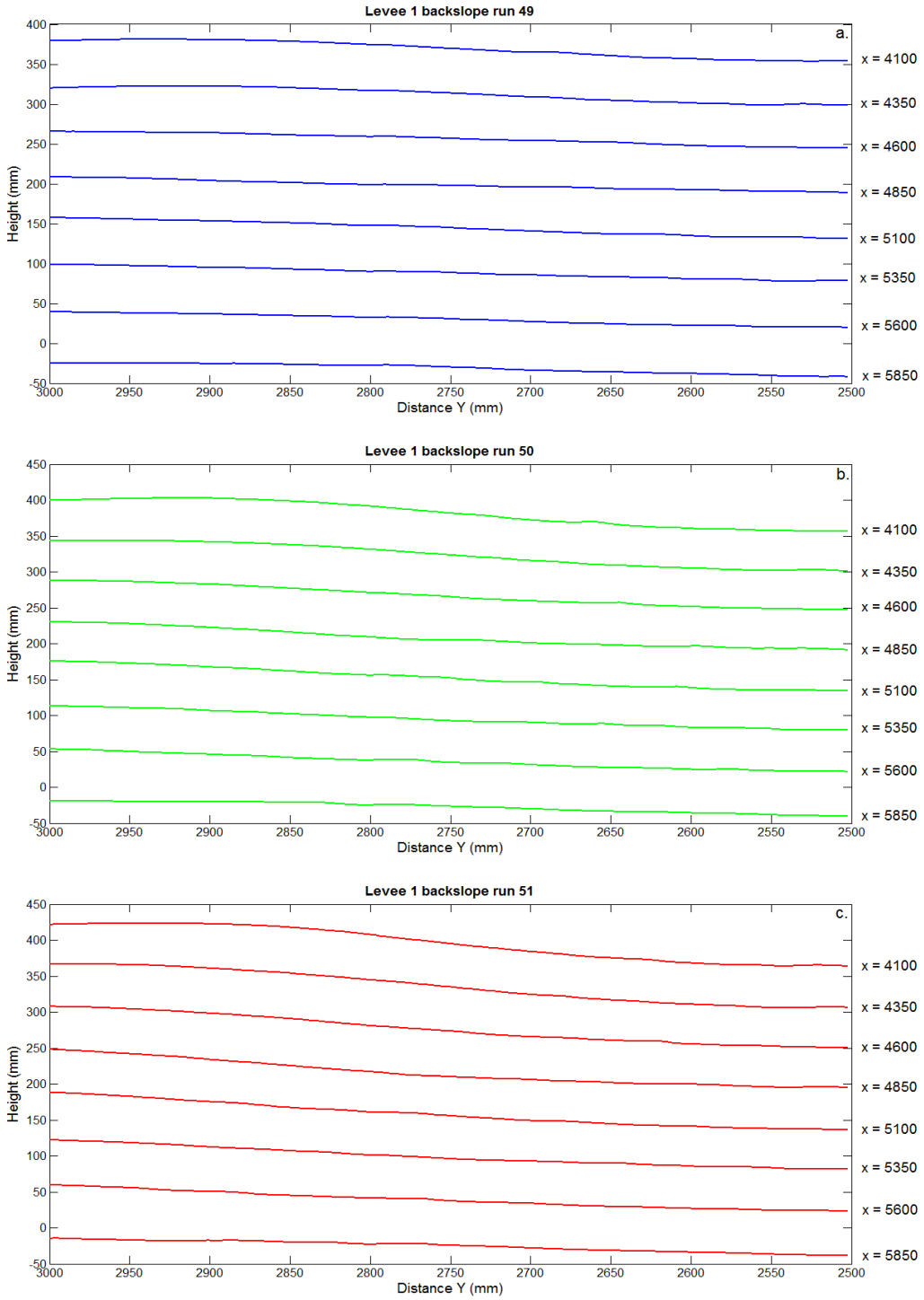

Figure 26: Backslope of levee 1 for all runs. Levee profiles have been taken from x = 4100 (upslope) to x = 5850 (downslope) in steps of 250 mm (as indicated at the right side of figure 26) . (a) Backslope run 49. (b) Backslope run 50. (c) Backslope run 51.

The backslope of run 49 (fig. 26a) shows a distinctive pattern in the shape of the profile along the slope which is strengthened in runs 50 (fig. 25b) and 51 (fig. 26c). Backslope profiles are curved upslope while the profiles are linear downslope. This pattern is best seen in figure 25c. These results show great resemblance with the results obtained by Straub and Mohrig (2008).

From these profiles the levee tapers can be calculated after each run. The definition and calculation of levee tapers is illustrated in figure 27. Heights y_1 and y_2, given in figure 27, are the total cumulative heights after each run. Levee tapers have been calculated for all runs at four locations (X = 4300, 4700, 5100 and 5500) and over a total interval (x) of 0.2 m, from Y = 2800 to Y = 2600 (see fig. 26).

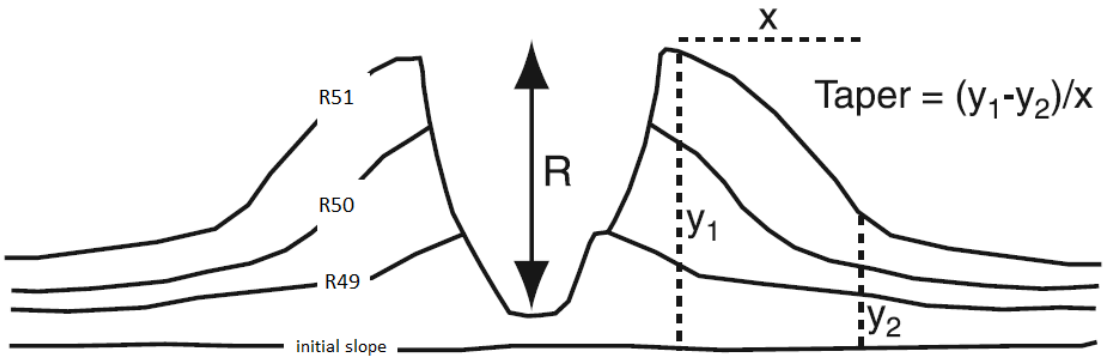

Figure 27: Sketch for the geometry of a levee (from Straub & Mohrig, 2008). In this study X = 0.2 m (from y = 2800 mm to y = 2600 mm). R = channel depth. Y_1 and Y_2 are the total cumulative heights.

Results of taper calculations are given in figure 28.

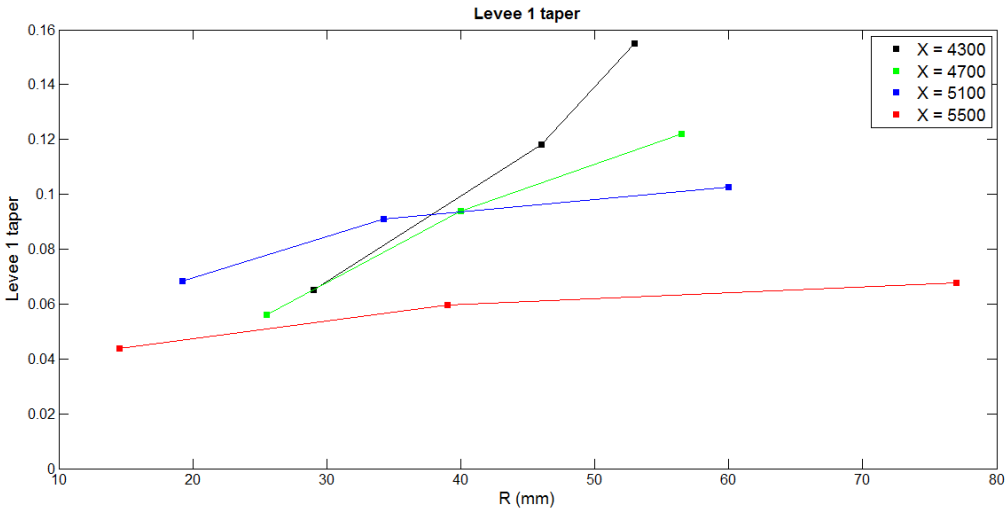

Figure 28: Taper results at x = 4300 (upslope), 4700, 5100 and 5500 (downslope). The growht rate of the taper decreases downlsope.

Upslope at X = 4300 levee taper increases exponentially with increasing relief. Further downslope (x = 4700 → x = 5500) levee taper decreases, and the growth rate of the taper decreases with increasing channel depth (R). The results obtained for levee tapers are in agreement with Straub & Mohrig (2008), Nakajima & Kneller (2013) and Ezz et al. (2014).

The results of taper calculations give insight about the shape of the levees and the way they were formed, in other words the morphodynamics of the levees. These implications are further elaborated in the discussion section of this report.

Comparison to naturally occurring systems

TRG Database

A comparison is made between naturally occurring systems (listed in the TRG database) and the experiments. This is done by comparing the channel depth/channel width ratio. The channel depth in the experiments is defined as the distance between the deepest point in the channel to the highest levee crest. The channel width is defined as the distance from levee crest to levee crest (see fig. 18). For the naturally occurring systems the mean values for channel depth and channel width are used.

Systems listed in the database which lack the necessary information (lateral or vertical channel dimensions) were not used. Therefore 76 of the 208 systems listed in the database had to be discarded, leaving 132 systems to be used for comparison. The dimensions of channel depth, and width of the experiments are obtained from cross-sections at x = 4600 and x = 4800. These have been picked because they are located at the lower part of the slope, which is less affected by the scour at the upper part of the slope. Also channel formation at these cross-sections represent a full path from an depositional state in run 49 to an erosional state in the latter runs.

Illustrated in figure 29 is the result of channel dimension comparison between systems listed in the database and the channel dimensions of this study at x = 4600 (channel dimensions extracted from the digital elevation models of each run at x = 4600). Illustrated in figure 30 is the outcome at x = 4800. Systems from the database are divided in 4 subdivisions, based on their main composition. These 4 subdivisions are gravel (in black), sand (in yellow), mud (in purple) and a mixture of sand and mud (in red). The width/depth (W/H) ratio of the experiments (run 49: 51,2; run 50: 20,7; run 51: 9,6) are plotted in the left bottom corner of the graph. These ratios are projected (solid lines) throughout the graph so that they can be compared with the systems listed in the database.

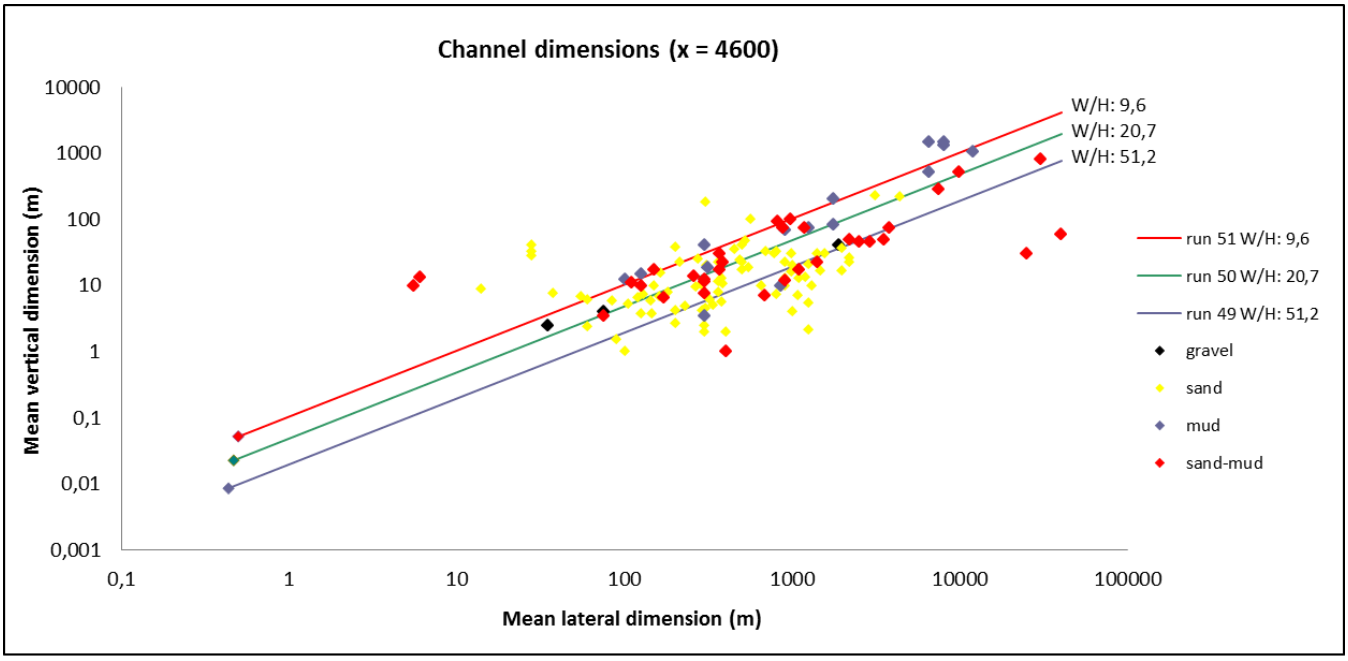

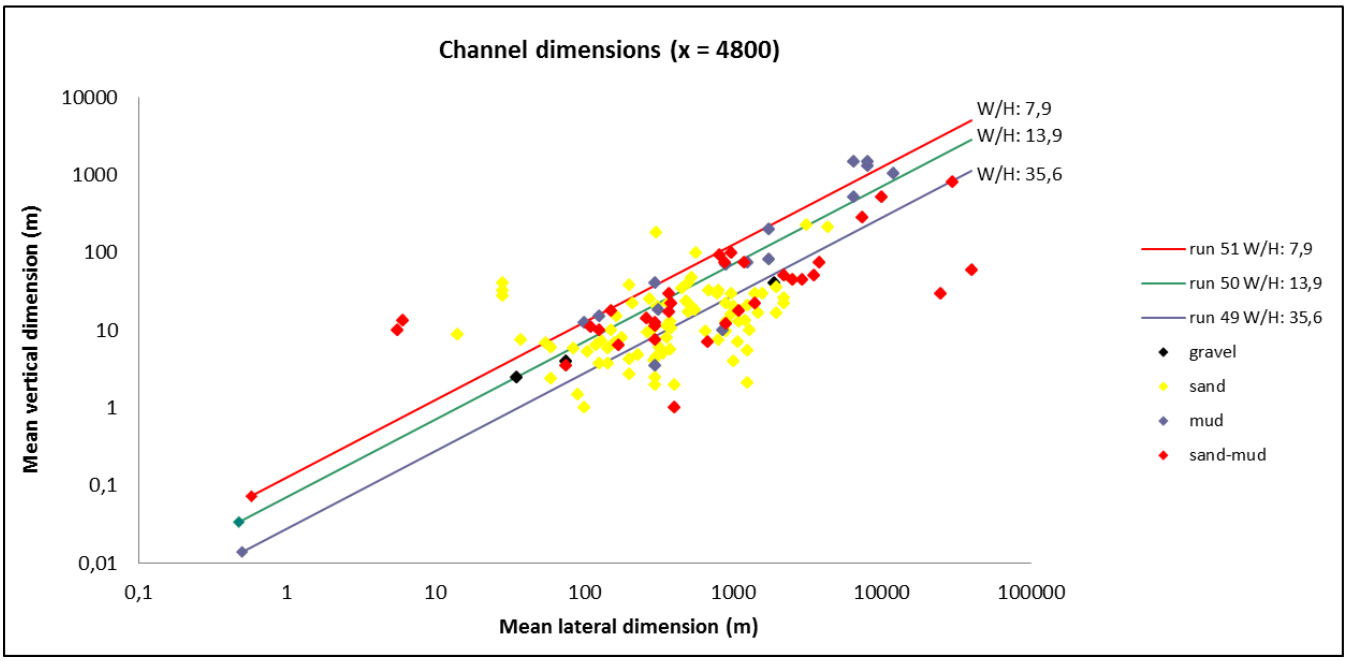

Figure 29: Upper graph. Channel dimensions (width/height ratio) for runs 49 – 51 and natural turbidity sytems listed in the TRG database at x = 4600. Ratios of each run are extended through the graph. Run 49 is indicated in blue, run 50 in green and run 51 in light-red. Width/height ratios of all runs are plotted in the graph. The natural turbidite systems are divided into 4 categories: gravel (in black), sand (in yellow), mud (in purple) and sand-mud (in dark-red).

Figure 30: Lower graph. Channel dimensions (width/height ratio) for runs 49 – 51 and natural turbidity sytems listed in the TRG database at x = 4800.

No distinct pattern can be recognized in the naturally occurring systems of the TRG database. In general it seems that muddy systems (purple) have a lower channel width/height ratio. The other systems (gravel, sand, sand-mud) do not show any clear pattern. The experiments (run 49-51) conducted in this study do show a pattern. An overall trend from run 49 to run 51 is a decrease in channel width/height ratio, and therefore a shift from broad, shallow channels towards narrow, deeper channels. An interesting observation is that the W/D ratio during the experiments is constantly changing while the systems from the database show a statistical end value. This will be further elaborated in the discussion section of this report.

The statistical end values of runs 49-51 show geometrical similarities with particular systems from the database. These geometrical similarities are based on shared channel width/height ratios of the experiments with the database systems.

Run 49 shows geometrical similarities with the Hueneme Fan formation, part of the Hueneme system, located in the Santa Monica basin (Los Angeles County, USA) and to the Brushy Canyon Fm, part of the FAN 7 system, located in Brushy Canyon (Texas, USA).

Run 50 shows geometrical similarities with the Gres d'Annot Formation, part of the Annot Turbidite System, located in Trois Eveches area (SE France).

Run 51 shows geometrical similarities with several formations in Brushy Canyon, part of the FAN 4 and 7 system, located in Brushy Canyon (Texas, USA).

A new interesting question arises from these similarities. What type of system relates to the experiments in this study? In order to answer this questions each system will be briefly described to sketch an image.

One of the key elements of this study was to create HDTC consisting only out of sand particles. The systems which have geometrical similarities are described as sand rich or sand-mud systems. The Heuneme system is described in the database as a sand-mud system. The Brushy Canyon formations as well as the Gres d'Annot Formation are described as sand rich systems. This is in good agreement with the experiments conducted in this study, which were conducted using only sand particles.

The Hueneme system and fan formations have been described by several authors. The studies that will be used here are from Normark et al. (1998), Piper et al. (1999) and Reynolds (1987).

The Hueneme fan is one of the largest sandy submarine fans filling the Santa Monica Basin. The basin has been a stable depocentre since the Pliocene (Vedder, 1987; Teng & Gorsline, 1989). The Santa Monica Basin has a water depth of just shallower than 1000 m. This water depth is relatively shallow compared to most deep-sea fans. Sand is transported towards the basin throug longshore currents until it is intercepted by a submarine canyon at the downdrift of a littoral cell. Mud is transported into the sytem during storms when mud on the shelf is resuspended by storm waves.

It is thought that sea-level fluctuations have a pronounced effect on the composition of the turbidity current and the morphology of the channel and levees. During lowstands initiation of turbidity currents resulted either from sediment failure during delta progradation or from hyperpycnal flows during floods, originating from the Santa Clara River. These flows contained a significant amount of mud with sand and are relatively efficient in carrying its content far into the basin (Mutti, 1979). These lowstand turbidity currents were most likely rich in mud, quite thick and had a long duration (perhaps days). These flows are responsible for rapid progradation and the maintenance of high levees. it is also believed that during glacials (lowstands) the amount of precipitation in this area was higher but conditions were still arid. Therefore the amount of sediment input by rivers is significantly higher, leading to more frequent turbidity currents.

During highstands the initiation of turbidity currents resulted from major earthquakes and exceptional river floods. There is more segregation of the delivery of mud and sand towards the basin. Due to this segregation the turbidity flows become less efficient and do not reach as far into the basin as during lowstands. As a result the width of the Hueneme fan is reduced from 2-3 km to 1 km, and much smaller inner levees are deposited within the broad channel which was formed during lowstands. The change in turbidity current characteristics is related to the Holocene sea-level rise.

The flow properties (velocity and density) of a turbidity current event in 1884 in the Hueneme fan were reconstructed in an article by Reynolds (1987). The velocity was determined to be 0.75 m/s but ranged from 0.1 to 0.9 m/s. The density was set at 4 kg/m^3 but ranged from 1 to 5 kg/m^3. The calculated velocity is slightly higher than the velocity measured in this study (table 1). The density is however much higher than the calculated density in this study. The density in this study was calculated using the "integral method" of Parker et al. (1987) in which the concentration profiles of the turbidity current is needed. These profiles were estimated for the experiments in this study which might explain the deviating density values of the Hueneme turbidity current and our experiments.

Deposits of the Brushy Canyon Formations have been described by Barton et al. (2007), Beaubouef and Rossen (2007), Gardner and Borer (2003) and Pyles et al. (2010).

The formations found at Brushy Canyon are part of a complex basin-floor-fan system with a complicated sinous channel network. Turbidite channels are oriented in multiple directions and are often truncated in several smaller channels which cross-cut each other. It is thought that the area was formed by an alternation of channelized and nonchannelized flows. There is no distinctive deposition of levees on the banks of the channel. Channel morphology originated from incision by turbidity currents into older sheet complexes. These sheet units were deposited by the nonchannelized flows in which deposition occurs over a broad area in a lobe-type structure. These sheets are then incised by the channelized flows which formed the sinous channel network. The sheet complexes as well as the channel complex consists out of well-sorted fine grained sandstones/conglomerates. Also distinctive for this system is the alternation between bypassing and depositional density currents which flowed through the channels. This lead to a process of repetative filling and incision of the channel. This alternation between bypassing and deposition are probably related to the consistency of the density currents. Eventually the system was abandoned and was covered with fine, deep-marine material (siltstone). These phases of abondanment were also alternated with phases of reinitiation before full abandonment.

The Gres d'Annot Formation has been described in detail by Etienne et al. (2012).

Sedimentary processes in the Trois Evêchés area were dominated by hyperconcentrated to concentrated flows (high-density turbidity currents) alternated with low-density turbidity currents (related to surge-type flows). Seven lithofacies were recognized based on grain-size and small-scale sedimentary structures. Facies 1 to 5 consist out of very coarse (microconglomerate) to fine grained sandstones which are all formed by high-density turbidity currents. Facies 6 and 7 were formed by low-density turbidity currents. This suggests an alternation of tubidity currents of high- and low-density.

Five main types of architectural elements were identified. Gravelly-filled channel-elements, laterally stacked channel-elements (which are interpreted as being relate to sinuous channel migrations) and wing-like channel-elements from the channelized sheet systems. Tabular sandstones, prograding and/or dome-shaped units constitute layered sheet systems. The sinuous channels are represented by the association of erosive-based, laterally stacked bedsets and very coarse, low-angle cross-bedded facies. These facies are the result of flow deconfinement and overbanks above channel margins. A conceptual model of the distribution and organisation of the components has been made

by making stratigraphic relationships between the five architectural elements. The model consists of proximal confined units were channelization processes, amalgamation and bypass dominates to distal and less confined units where compensation, constructive structures and high deposition rates control sedimentary architectures.

Discussion

The short summaries of the Hueneme, Gres d'Annot and Brushy Canyon turbidite systems show some aspects which are very similar such as: grain size, density of the turbidity current (high density) and flow velocity of the current (Hueneme system). There are however also many different fundamental aspects which are present in these systems but lacking in the experiments of this study. One of these aspects is sea-level fluctuation by which all naturally occurring systems have been affected through time. If we want to relate the results of our experiments with these systems than this should be taken into account. It is evident that fluctuation in sea-level could have a pronounced effect on turbidite systems. During periods of lowstand sea-level drops beneath the shelf while during periods of highstand the shelf is flooded. Sea-level fluctuations also affect the characteristics of river delta's (progradation/aggradation). These processes must have modified the composition (sand-mud ratio) of turbidity currents through time, which is also described in the article of Normark et al. (1998) about the Heuneme turbidite system. The composition of sediment which source turbidity currents is not only affected by sea-level fluctuations but also by climate change and tectonics. Changes in climate can alter the amount of precipitation and whether an area is arid or moist. This again alters the amount of erosion on land and therefore the sediment composition of river discharge. Tectonics can alter sediment composition by uplift or subsidence near turbidite systems.

Another aspect which was not taken into account in the experiments is the influence of different sediment input directions. In naturally occurring systems the influx of sediment often comes from different orientations. Variations in input orientation alters the morphology of channel systems (cross cutting of channels) which is also described in an article by Beaubouef and Rossen (2007) about the Brushy Canyon turbidite system.

Also incision into sheet complexes or lobe deposits was not incorporated in this study. In naturally occurring systems this is often the case, in which a turbidity current starts to incise in these deposits which were formed by prior density currents. During this study this was deliberately avoided by creating a height difference at the toe of the slope. This prevented the generated turbidity currents to reach the lobe, and prevented backstepping of the lobe onto the slope.

In future experiments these aspects need to be incorporated in flume experiments if we truly want to simulate and investigate the processes which govern naturally occurring turbidity currents. The

main goal in future experiments should be to use a variety of sediment compositions as it is relatively easy to incorporate, and seems to have a large influence on the morphology of turbidite initiated channels and levees.

It should also be questioned whether a direct comparison can be made between flume experiments and the statistical 'end' values of natural turbidite systems (such as listed in the TRG database). The statistical end values, listed in the database, of turbidite systems are taken from abandoned systems or represent a snapshot in the evolution of a (still active) turbidite system. The abandonment of a system can occur at any moment in its evolution, the same applies for the snapshot. Therefore a straightforward comparison between flume experiments and natural turbidity systems is unrealistic. Perhaps it is even unrealistic to relate these to each other. All turbidity systems, whether created in flume experiments or naturally occurring systems, undergoes constant transformation. These transformations can be caused by a constant series of similar turbidity currents flowing down a channel or by a variety of external factors (sediment composition, sea-level, input orientation etc.). Due to this constant change in factors, which influence the morphology of turbidity systems, any type of system anywhere on the world can show similar channel dimensions at some point in time to the flume experiments of this study.

Discussion

Velocity trends

Two velocity probe set-ups have been used to measure the velocity during the experiments (as described in the methods). The first set-up was used in runs 40-48, the second setup in runs 49-51. Velocity profiles obtained with the first set-up show a clear pattern in which the velocity decreases downslope due to expansion of the turbidity current, friction with the bed and resistance of the ambient fluid. Unfortunately no successful run was executed with this first set-up, in which a channel/levee system was formed. Run 44 can be described as semi-successful (fig. 4). A slight increase in velocity (fig. 5) from probe 2 to probe 3 was measured during this experiment.

The probes measuring the downslope velocity in the second set-up show a pattern of a decrease in velocity from the channel towards the sides of the slope. The highest velocities are reached in the channel, velocities on top of the levees are lower but still significant. The lowest velocities are measured at the edge of the slope. Velocities in the channel increase after each run (runs 49-51) while the velocity measured on top of levee 1 is more or less constant (slight decrease) (fig. 20 - 22). Velocities measured at the edge of the slope (probe 5) decrease after each run. These patterns in velocities must be caused by changes in morphology as the initial conditions (e.g. initial discharge) were held constant. The main processes which can affect turbidity currents are changes in slope gradient and confinement of the flow.

Slope gradient

The channel gradient (fig. 23) at the position of velocity measurements increases from 12.3° (run 49) to 13.1° (run 50) to 14.3° (run 51). It is considered that changes in slope have a large effect on the mean- and maximum velocity (M. Hofstra, 2013), therefore it is plausible that this increase in gradient could lead to increasing velocities in the channel. The same process should apply to the velocity measured at the crest of levee 1 (probe 4). Figure 24 shows no significant changes in gradient at the position of velocity measurements, therefore velocities measured at probe 4 should be more or less constant. This is in agreement with the measurements (fig. 20 - 22) obtained by probe 4, which show no significant changes in velocity. The velocity measured at probe 5 (side of the slope) decreases in every consecutive run, which means that the gradient should decrease in every consecutive run as well. Figure 31 shows the slope gradient at probe 5.

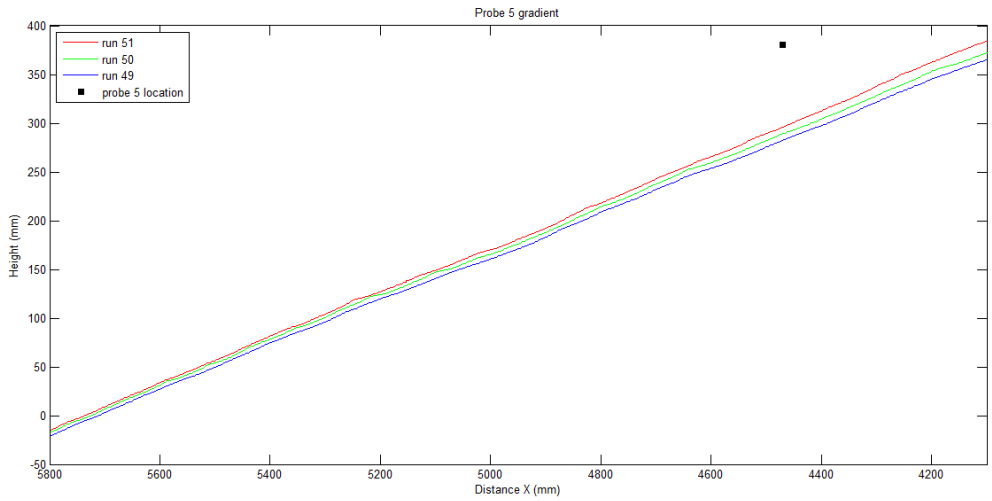

Figure 31: Gradient at probe 5.

The gradient at probe 5 slightly increases with every run, which means that velocities should have increased instead of decreasing. Therefore another process must be affecting the velocity of the turbidity current. As mentioned above, another process which can enhance the velocity in the channel and decrease the velocity outside the channel is confinement of the turbidity flow.

Confinement

The second main process which affects the velocity and behaviour of a turbidity current is confinement. Confinement is enhanced when channel depth increases and levee height increases. An extra stimulating factor for channel velocities is narrowing of the channel, which concentrates the flow through the channel.

Figure 25c shows an increasing channel depth over the entire length of the slope, the highest increase is reached at the low-end of the slope. Figures 25a shows an increase in the height of levee 1, especially at the probe location. The height of levee 2 also increases in each run (fig. 25b), the final height is however significantly lower than that of levee 1 and height increase from run 50 to run 51 is minimal. This hampers confinement of the flow by means of levee height increase. Due to the lower height of levee 2 overspilling of the flow can still occur at this side. Therefore the highest increase in channel velocity, which occurs from run 50 to run 51 (fig. 21a), has to be the result of the increase in channel depth rather than levee height increase. This transition can also be marked as the transition from aggradational confinement to incisional confinement. This trend of increasing velocity with increasing channel depth is also shown in figure 32, which shows the mean channel velocity and channel depth during all of the runs at the position of probe 1.

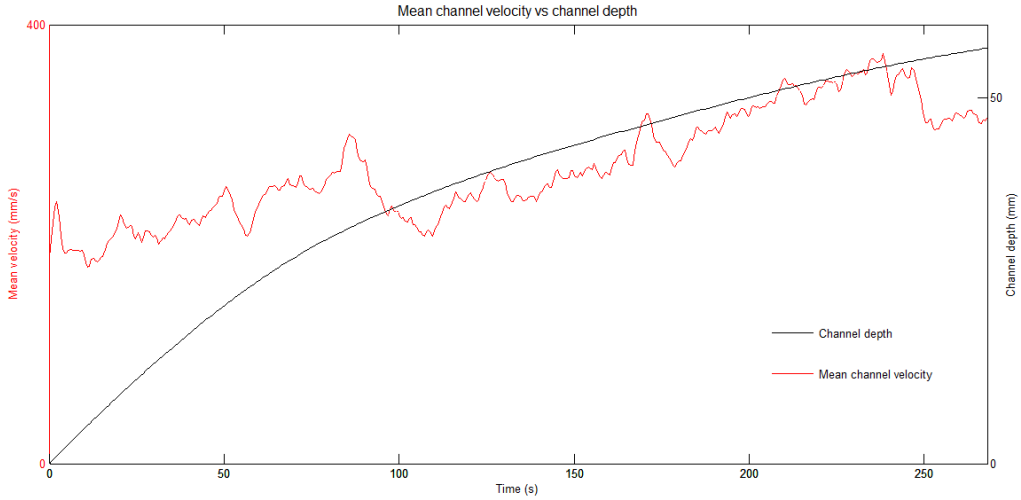

Figure 32: Mean channel velocity and channel depth with time at the position of probe 1 (x = 4470).

Confinement of the turbidity current could also be the cause for decreasing velocities at probe 5. Due to the confinement the current is concentrated through the channel, decreasing the amount of volume of the flow which reaches probe 5 which can lead to decreasing velocities.

There are however some problems with the process of confinement and its effect on the velocities measured by the probes. If the turbidity current is confined by an increasing channel depth and increasing levee heights, you would expect the velocities measured on top of levee 1 to decrease. This is however not the case, velocities measured on top of levee 1 (probe 4) remain more or less constant throughout the runs (fig. 20 - 22). Also the increase in mean channel velocity from run 49 to run 50 is very minimal (fig. 20 - 22) although the increase in channel depth and increase in levee heights is significant (fig. 25a,b,c). If confinement plays a major role in increasing the channel velocity you would expect that it would be visible from run 49 to run 50. The pattern of channel velocity throughout the runs shows more comparison with the channel gradient (fig. 23). The gradient barely increases from run 49 to run 50 (mean channel velocity barely increases from run 49 to run 50), and the gradient is significantly increased from run 50 to run 51 (mean channel velocity is significantly increased from run 50 to run 51). However the change in gradient cannot explain decreasing velocities at probe 5. This leads to the conclusion that both processes (confinement and fluctuating slope gradients) affect the velocity of the turbidity current. I propose that the gradient has the most pronounced effect on the channel velocities while confinement has a pronounced effect on the distribution of the turbidity current over the slope and concentrating the flow through the channel.

The velocity profile obtained by the probe 3, measuring the sideway velocity in the second set-up, shows an interesting pattern. As mentioned in the results section, red colours indicate velocities of the flow coming towards the probe, while blue colours indicate velocities of the flow moving away from the probe (fig. 12). If the velocity profile is indeed divided into an upper red part and a lower blue part this should be clearly visible in the time-averaged velocity profiles of probe 3. The time-averaged velocity in the lower part should be negative (blue part, flowing towards the channel) while the time-averaged velocity in the upper part should be positive (red part, flowing towards the levee). Figure 33 shows the time-averaged velocities of probe 3 for all of the runs.

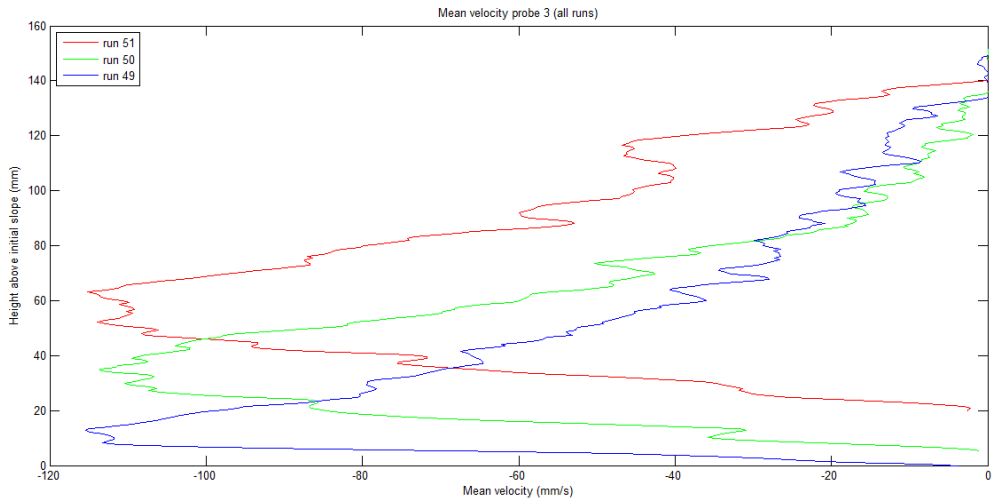

Figure 33: Mean velocities of probe 3 for all runs.

Only negative velocities are obtained by probe 3. This means that there is only flow towards the azimuth of the channel, especially at the bottom. This is probably related to flow of the current from levee crest towards the channel.

Agradational systems vs. incisional systems

A levee is an embankment alongside a channel which is produced naturally by sedimentation. In natural turbidity systems these levees are symmetrical to each other. In the digital elevation models of runs 49 - 51 (fig. 6, 8, 10) a segregation can be seen between an symmetrical lower part and a asymmetrical upper part. The levees become more symmetrical in each consecutive run, expanding the symmetrical part of the system. The asymmetrical upper part of the DEM's of runs 49-51 could be formed by expansion of the turbidity current after entering the tank. However, it could also be caused by the formation of a small scour in the channel (light blue spot) on the upper part of the slope. Because the lower part is rather symmetrical it is more likely that the upper part started out symmetrical as well and became asymmetrical during the experiment by the formation of the scour.

A widely accepted theory is that levees are formed, and develop further, due to overspilling of channelized turbidity currents (Rowland et al., 2010). This theory implies that a turbidity current should first incise into pre-existing strata to become channelized. After incision the formation of levees can be initiated. During this study turbidity currents were sent down an smooth slope with no sorts of channel morphology present. The digital elevation models and velocity profiles also do not show initial incision of the turbidity current into the slope during the experiments, from which the process of overspilling could be initiated. This raises the question of how the turbidity current becomes channelized (how does channel formation begins). To answer this question we must first define which type of channel has been formed in the experiments.

Clark and Pickering (1996) suggested the existence of three types of channel types in modern and ancient settings (fig. 34a). Maier et al. (2013) and others (e.g. Campion et al., 2000; Gardner & Borer, 2000; Schwarz & Arnott, 2007; McHarue et al., 2011) further suggested that each channel element records a phase of channel surface creation (erosion) followed by channel filling (deposition) to produce a sedimentary body with channel-form geometry in cross-section (fig. 34b). They suggest that depositional systems, as was described in the scheme of Clark and Pickering (fig. 34a), do not exist.

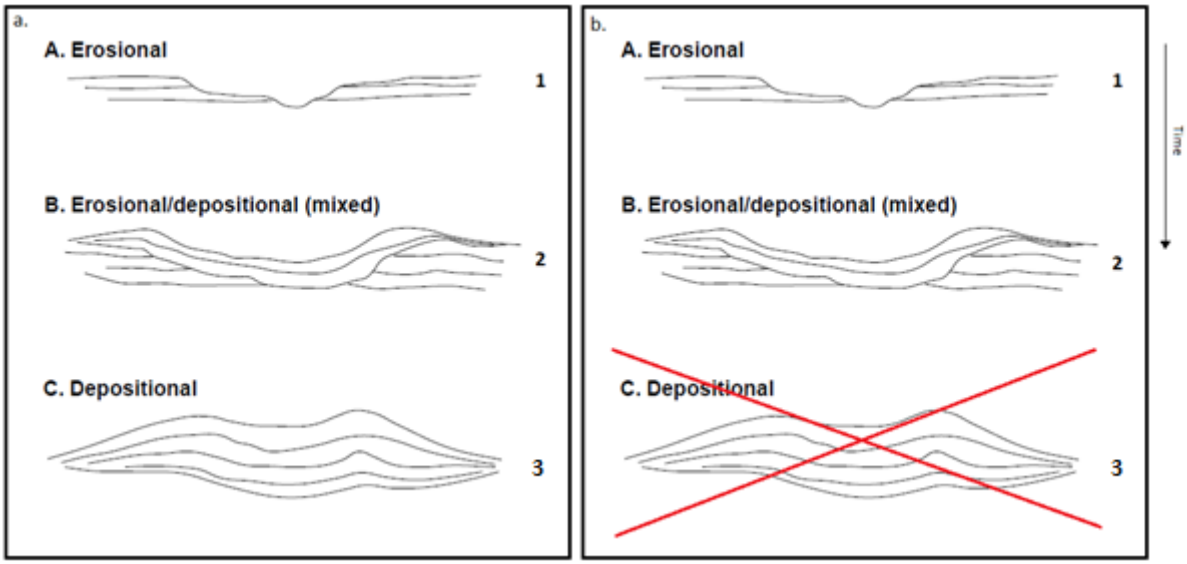

Figure 34: Channel type settings (from Clark and Pickering, 1995). (a) Main type of channel settings as suggested by Clark and Pickering (1995). (b) Main type of channel settings and evolution through time as suggested by Maier et al. (2013).

However, the experiments performed in this study show that depositional channel systems do exist. The DEM of run 49 (fig. 6) shows such a depositional system, where deposition occurs over the entire slope. More sediment is deposited at the sides than in the centre. This was also argued by Imran et al. (1998), in which he stated that net deposition along the margins of a sediment-laden flow must exceed that in the core of the flow. This process leads to channelization of the turbidity current and the formation of a channel and levees. Channel formation is initiated by deposition instead of incision. This is also visible in the cross-sections made from the digital elevation models (fig. 14 - 17), in which run 49 clearly shows a depositional system. After multiple runs have been carried out a transition occurs. The system gradually changes from a depositional system towards an erosional/depositional (mixed) system. This is also well visible from the cross-sections. This implies that the formation of a channel/levee system can start with a depositional system (nr. 3) which gradually changes into an erosional/depositional system (nr. 2) as turbidity currents keep flowing. This does not mean that channel/levee systems can not originate from erosional systems (nr. 1) towards erosional/depositional systems (nr. 2), but depositional systems should not be excluded. The lack of depositional systems in ancient deposits can be explained due to the fact that depositional systems are short-lived systems which change into erosional/depositional systems over time. How such depositional systems are formed remains uncertain. A theory is suggested by Johnson et al. (2012) in which he suggests that grain-size segregation occurs within a turbidity current in which the coarser fraction is transported to the margins of the current. Because the kinematic energy at the margins is lower than in the centre this coarser fraction is deposited at the margins. This leads to a net difference in deposition between the margins and the centre and channelization of the flow. It is

most likely that the flow in the centre of the turbidity current is higher than at the side, therefore deposition could occur at the sides. After the flow becomes more channelized, velocities in the channel increase and incision in the channel can occur. This causes the transition from depositional systems towards erosional/depositional systems.

Backslope

The shape of the backslope of levee 1 (fig. 26) and the taper calculations at x = 4300, 4700, 5100 and 5500 (fig. 28) are in good agreement with previous studies (e.g. Straub & Mohrig, 2008; Nakajima & Kneller, 2013; Ezz et al., 2014). The results in these previous studies were obtained from flume experiments (also in this study) but also from naturally occurring systems (e.g. channel network offshore Brunei). This agreement in results between the flume experiments conducted in this study and naturally occurring systems means that the natural processes which influence turbidity currents can be simulated in flume experiments.

The recognizable shape of the backslope of levee 1 (fig. 26), which shows power-law decay upslope and shifts towards exponential decay moving downslope, can be explained by the amount of overspilling of the turbidity current. This theory has been suggested by Straub and Mohrig (2008) and is also applicable to this study. Due to the loss of sediment as the current flows down the slope the height of the current also decreases. As a consequence there will be less overspilling downslope and the overspilling will consist out of increasingly finer fractions of the sediment. This means that upslope more coarse material will settle down on the levee and downslope more fine material. This results in more thicker levees upslope which rapidly decrease (power-law decay) towards the side and more shallow levees downslope which are more draped towards the side (exponential decay).

This same process explains the taper results as well (fig.28). Due to the build-up of levee 1 the amount of overspilling decreases with each run. This leads to decreasing taper results and smoother taper profiles (fig. 25). This process is well explained in figure 35.

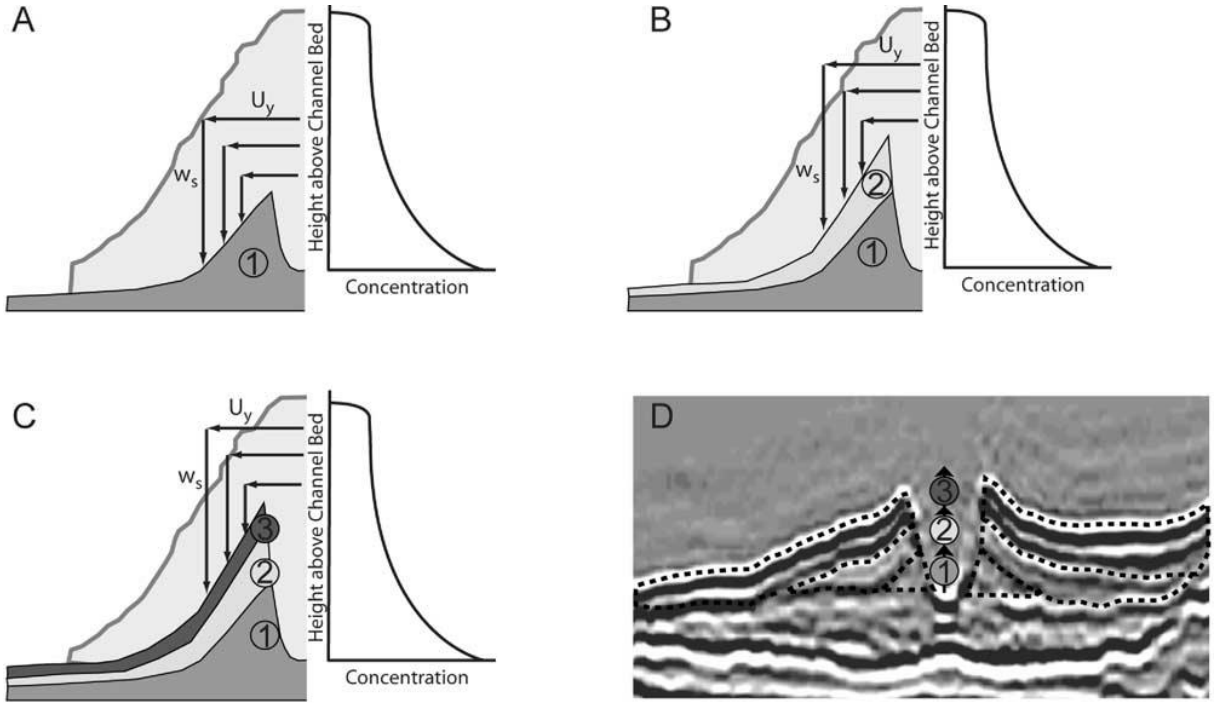

Figure 35: Schematic diagrams from Struab and Mohrig (2008) showing the evolution of levee morphology for bypassing turbidity currents. (a) Initial channel formation and growth is associated with rapid increase in bulk levee taper as high amounts of suspended sediment is able to exti the channel. (b) As levee relief increased due to deposition less overspilling occurs and increasingly finer fractions of the suspended sediment will be able to exit the channel resulting in a decreasing taper. (c) As channel depth aproaches current height only the finest fractions will be able to spill over the overbank resulting in even lower tapers. (d) Seismic section from a channel offshore Brunei which shows similar results.

Key to succes and future experiment improvement

The key to success for these experiments was the constant change of boundary parameters until a successful run was executed. Hereafter the parameters were kept constant. Boundary parameters which could be adjusted are: concentration, composition, discharge and slope gradient. The parameters for each run (successful and unsuccessful) are listed again in table 3. The final key to success was the adjustment of composition. In the final runs only the finer fractions were used. By removing the coarser fractions, which deposit relatively fast, the current became more efficient. It is however still unclear what the precise boundary parameters settings should be for success. In the final runs, from 47 till 51, the discharge also seems to have a large effect on the deposition. It seems that lowering the discharge was also a key element for success but after evaluating the digital elevation models of run 47 and run 48 (appendix A) this is not so evident. Run 47 seems to be closer related to a system which can be called a 'turbidite system' than run 48. But in the end, lowering the discharge even further (to 30 m^3/h) brought final success. This raises some doubt in what exactly the key to success should be. However, future experiments (with a similar set-up) should keep the boundary parameters of run 49 - 51 in mind.

Table 3: Experimental boundary parameters

Run	Con (%)	Comp. (µm) *	Discharge (m^3/h)	Slope gradient (°)
41	13,4	2:3:1:1	20	10
42	13,1	2:3:1:1	50	10
43	13,1	2:3:1:1	45	10
44	13,3	2:3:1:1	50	11
45	13,4	2:3:1:1	50	12
46	17	2:3:1:1	50	12
47	16,8	1:1:0:0	45	12
48	16,9	1:1:0:0	33	12
49	17,3	1:1:0:0	30	12
50	16,8	1:1:0:0	30	12
51	17,4	1:1:0:0	30	12

Successful

Unsuccessful

Further improvements for future Eurotank flume experiments should be to incorporate more UVP's in the experiment set-up. During this study velocity profiles could only be measured lateral or along the axis of the slope. In the successful runs only lateral velocity profiles were obtained. This was very useful for interpreting the context of the velocity within the channel and outside the channel, but it would also be useful to observe this context along the axis of the slope within the channel. Channel

confinement seems to be further developed downslope than uplsope, and it would be interesting to observe if this has any consequences on the velocity within the channel as well. Therefore more UVP's are needed to better constrain the effect of confinement on current velocity and processes. Elements which should be incorporated to further improve the realistic aspect of flume experiments, and to improve the analogy between these experiments and natural turbidite systems are: usage of different sediment compositions and incorporation of lobe deposits. As discussed earlier the sediment composition of natural turbidity currents change over time in the same system. This seems to have a big effect on the properties of the current and the resulting morphology. Also the presence of a lobe at the toe of the slope has a pronounced effect on turbidity current processes. It should however be kept in mind that during this study only a small segment of a slope turbidite system was recreated, therefore the incorporation of a lobe is not absolutely necessary. It depends on which segment of the slope is preferred to be recreated.

Conclusion

A series of 3D flume experiments were executed to study the evolution of a turbidite system in relation with the flow dynamics of high-density turbidity currents. During these experiments several boundary parameters (concentration, sediment composition, discharge and slope gradient) were varied in order to successfully simulate a turbidite channel - levee system in the laboratory. The key to succes is, despite careful logging of the boundary parameters, not fully understood. Success was however achieved (runs 49 - 51) and the corresponding boundary parameters (table 2) should be used in future flume experiments with a similar set-up.

The channel dimensions (width/height ratio) of the results of this study were related to natural occurring systems (listed in the TRG database). Similarities were found between the results and the Gres d'Annot, Brushy Canyon and Heuneme systems in grain size, density of the turbidity current (high density) and flow velocity. However, some fundamental differences were also observed. In natural systems the sediment composition of turbidity currents in one system alternates over time (sand - mud ratio). Although the main composition of the related natural systems is similar, these natural systems still show segments of difference in sediment composition. These differences are most likely caused by sea-level fluctuations, climate change or tectonics. Further differences are varying sediment input orientations and incorporation of lobe deposits into the experiments. By incorporating these elements into future flume experiments a more realistic result will be achieved. It should also be questioned whether a direct comparison can be made between flume experiments and natural turbidity systems. The statistical end values of the natural systems (listed in the TRG database) represent abandoned systems or a snapshot in the evolution of a system. It should be

emphasized that both natural systems and the results of the flume experiments undergoes constant change due to the natural evolution of a system or varying external factors. Due to this constant change in factors, which influence the morphology of turbidity systems, any type of system anywhere on the world can show similar channel dimensions at some point in time to the flume experiments of this study.

The velocity profiles obtained during this study show a clear pattern of increasing velocities inside the channel and decreasing velocities outside the channel. After evaluation of both slope gradient and confinement of the turbidity current, by means of increasing levee heights and channel depth, it is concluded that both factors are responsible for the observed velocity pattern. I propose that increasing confinement of the current is responsible for decreasing velocities outside the channel by concentrating the current through the channel. The increasing slope gradient inside the channel is the main contributing factor for the increasing velocities inside the channel.

The turbidite system created in this study started as a depositional system and shifted towards a erosional/depositional system (as described by Clark and Pickering, 1996). The fact that this system started out as a depositional system contradicts the suggestions of Maier et al. (2013) and others (e.g. Campion et al., 2000; Gardner & Borer, 2000; Schwarz & Arnott, 2007; McHarue et al., 2011) which state that such systems do not exist. Channel formation was initiated by deposition which lead to channelization of the turbidity current and formation of a channel with accompanying levees. A prerequisite is that net deposition along the margins of a sediment-laden flow must exceed that in the core of the flow, which is visible in the digital elevation models of this study. The conception behind this process is still not understood, although some authors are suggesting theories (e.g. Johnson et al., 2012). After channelization of the flow, velocities in the channel increase and incision in the channel increases. This leads to the transition from an depositional system towards an erosional/depositional system.

The shape of the backslope of levee 1 across the slope is in good agreement with previous flume experiments and natural turbidite systems (e.g. Straub & Mohrig, 2008; Nakajima & Kneller, 2013; Ezz et al., 2014). The recognizable shape of the backslope, which shows power-law decay upslope and shifts towards exponential decay moving downslope, can be explained by the amount of overspilling of the turbidity current (Straub and Mohrig, 2008). The increase in channel depth downslope (by incision or increasing levee height) causes less overspilling and causes the overspill to consist out of an increasingly finer fraction of the sediment (fig. 35).

Acknowledgments

For the success of this project I would like to thank:

Dr. J. T. Eggenhuisen for the opportunity to write my master thesis under his outstanding, patient and enthusiastic supervision. But also for the opportunity to execute my experiments in the Eurotank laboratory.

J. de Leeuw for the preparation of the experiment, his constant supervision during the experiments, many useful tips for the experimental set-up, infinite help in decoding the MATLAB mystery program and many fruitful discussions about the subject. I can definitely say that without Jan this thesis would not have been possible.

T. van der Gon Netscher for supplying all materials and equipment and his efficient way of solving experimental problems

H. van de Meer for taking care of all ICT problems with the equipment.

P. Michielsen for all the laughs and good times in- and outside the laboratory. Many beers were consumed.

H. Woolderink for all his hard work in shovelling sand around the lab.

And last but certainly not least my mother and father, to whom I owe everything.

References

Abreu, V., Sullivan, M., Pirmez, C. & Mohrig, D. 2003, "Lateral accretion packages (LAPs): an important reservoir element in deep water sinuous channels", Marine and Petroleum Geology, vol. 20, no. 6, pp. 631-648.

Adeogba, A.A., McHargue, T.R. & Graham, S.A. 2005, "Transient fan architecture and depositional controls from near-surface 3-D seismic data, Niger Delta continental slope", *AAPG Bulletin,* vol. 89, no. 5, pp. 627-643.

Agirrezabala, L. M. and Garcia, M. J. 1994. A coarse grained turbidite system with morphotectonic control (middle Albian, Ondarroa, northern Iberia). Sedimentology 41(3): 383-407.

Antobreh, A.A. & Krastel, S. 2006, "Morphology, seismic characteristics and development of Cap Timiris Canyon, offshore Mauritania: a newly discovered canyon preserved-off a major arid climatic region", *Marine and Petroleum Geology,* vol. 23, no. 1, pp. 37-59.

Arnott, R. 2007, "Architecture of lateral-accretion deposits in two stacked, deep-water, sinuous channel fills: Relationship between coarse channel-fill and adjacent inner-bend levee deposits, Isaac channel 2, Castle Creek South, Windermere Supergroup, British Columbia, Canada", *Atlas of deep-water outcrops: AAPG Studies in Geology,* vol. 56, pp. 89-92.

Arnott, R. 2007, "Stratigraphic architecture and depositional evolution of a levee to proximal crevasse-splay to channel-fill succession: Units 13 and 14, Castle Creek North, Isaac Formation, Windermere Supergroup, British Columbia, Canada", *Atlas of deep-water outcrops: AAPG Studies in Geology,* vol. 56, pp. 111-114.

Baas, J.H., McCaffrey, W.D. & Knipe, R.J. 2005, "The Deep-Water Architecture Knowledge Base: towards an objective comparison of deep-marine sedimentary systems", *Petroleum Geoscience,* vol. 11, no. 4, pp. 309-320.

Babonneau, N., Savoye, B., Cremer, M. & Klein, B. 2002, "Morphology and architecture of the present canyon and channel system of the Zaire deep-sea fan", *Marine and Petroleum Geology,* vol. 19, no. 4, pp. 445-467.

Barton, M. D., O'Byrne, C. J. and Pirmez, C. 2007. Facies architecture of a deep-water fan valley, Plane Crash Canyon, Brushy Canyon Formation, Texas, USA. In: Nilsen, T. H., Shew, R. D., Steffens, G. S. and Studlick, J. R. J. (Eds). Atlas of Deep-Water Outcrops. AAPG Studies in Geology 56: 445-449.

Barton, M., O'Byrne, C., Prather, B., Pirmez, C., Sylvester, Z. & Commins, D. 2007, "Deep-water channel-complex architecture, Popo fault block, Brushy Canyon Formation, Texas, USA: Part 2. Facies architecture", *Atlas of deep-water outcrops: AAPG Studies in Geology,* vol. 56, pp. 463-466.

Barton, M., O'Byrne, C., Steffens, G., Pirmez, C. & Buergisser, H. 2007, "Architecture of an aggradational deep-water channel complex: Channel complex 2, Isaac Formation, Windermere Supergroup, British Columbia, Canada", *Atlas of deep-water outcrops: AAPG Studies in Geology,* vol. 56, pp. 106-110.

Barton, M., Steffens, G. & O'byrne, C. 2007, "Facies architecture of a submarine-slope channel complex, Condor West channel, Cerro Toro Formation, Chile", *Atlas of Deep-Water Outcrops, American Association of Petroleum Geologists, Studies in Geology,* vol. 56, pp. 149-153.

Barton, M.D. & Dutton, S.P. 1999, "Outcrop analysis of a sand-rich, basin-floor turbidite system, Permian Bell Canyon Formation, west Texas", *Transactions, Gulf Coast Section SEPM 19th Annual Bob F. Perkins Research Conference, December*SEPM, , pp. 53.

Basilici, G. 2006, "Depositional mechanisms and architecture of a pre-early Cambrian mixed sand–mud deepwater ramp (Apiúna Unit, South Brazil)", *Sedimentary Geology,* vol. 187, no. 3, pp. 183-204.

Beaubouef, R. T. and Rossen, C. 2007. Basin-floor channel and sheet complexes of the Colleen Canyon area, Lower Brushy Canyon Formation, Texas, USA. In: Nilsen, T. H., Shew, R. D., Steffens, G. S. and Studlick, J. R. J. (Eds). Atlas of Deep-Water Outcrops. AAPG Studies in Geology 56: 467-470.

Beaubouef, R., Rossen, C. & Lovell, R. 2007, "The Beacon Channel: a newly recognized architectural type in the Brushy Canyon Formation, Texas, USA", *Atlas of deep-water outcrops: AAPG Studies in Geology,* vol. 56, pp. 432-443.

Bouma, A. H., Delery, A. M. and Scott, E. D. 2007. Base-of-slope channel deposits, Ongeluks River Farm, Tanqua Karoo, South Africa. In: Nilsen, T. H., Shew, R. D., Steffens, G. S. and Studlick, J. R. J. (Eds). Atlas of Deep-Water Outcrops. AAPG Studies in Geology 56: 305-306.

Bouma, A. H., Delery, A. M. and Scott, E. D. 2007. Channel and levee deposits, Bloukop Farm, Tanqua Karoo, South Africa. In: Nilsen, T. H., Shew, R. D., Steffens, G. S. and Studlick, J. R. J. (Eds). Atlas of Deep-Water Outcrops. AAPG Studies in Geology 56: 307-310.

Bouma, A. H., Delery, A. M. and Scott, E. D. 2007. Kanaalkop channel complex, Kleine Gemsbok Fontein Farm, Tanqua Karoo, South Africa. In: Nilsen, T. H., Shew, R. D., Steffens, G. S. and Studlick, J. R. J. (Eds). Atlas of Deep-Water Outcrops. AAPG Studies in Geology 56: 311-313.

Brandes, C., Struss, I., Vandre, C. and Winsemann, J. 2007. Architecture of proximal midfan levee deposits, Punta Farallones La Flor, Nicaragua.In: Nilsen, T. H., Shew, R. D., Steffens, G. S. and Studlick, J. R. J. (Eds). Atlas of Deep-Water Outcrops. AAPG Studies in Geology 56: 271-273.

Browne, G., King, P., Arnot, M. & Slatt, R. 2007, "Architecture of base-of-slope fans, Mount Messenger Formation, Pukearuhe Beach, New Zealand", *Atlas of deep-water outcrops: AAPG Studies in Geology,* vol. 56, pp. 257-261.

Bruhn, C.H. & Walker, R.G. 1997, "Internal architecture and sedimentary evolution of coarse-grained, turbidite channel-levee complexes, Early Eocene Regencia Canyon, Espirito Santo Basin, Brazil", *Sedimentology,* vol. 44, no. 1, pp. 17-46.

Busby Spera, C. J. 1985. A sand-rich submarine fan in the lower Mesozoic Mineral King Caldera Complex, Sierra Nevada, California.Journal of Sedimentary Petrology 55(3): 376-391.

Campion, K. M., Sprague, A. R. and Sullivan, M. D. 2007. Architecture and lithofacies of the Miocene Capistrano Formation, San Clemente State Beach, California, USA. In: Nilsen, T. H., Shew, R. D., Steffens, G. S. and Studlick, J. R. J. (Eds). Atlas of Deep-Water Outcrops. AAPG Studies in Geology 56: 395-400.

Campion, Kirt M., et al. 2000 "Outcrop expression of confined channel complexes."Deep-Water Reservoirs of the World, SEPM, Gulf Coast Section, 20th Annual Research Conference.

Cavuoto, G., Valente, A., Nardi, G., Martelli, L. & Cammarosano, A. 2007, "A prograding Miocene turbidite system, Tempa Rossa Cliffs, Italy", *Atlas of deep-water outcrops: AAPG Studies in Geology,* vol. 56, pp. 218-221.

Chapin, M. A. 2007. Amalgamated sheet and channel sandstones at Kilbaha Bay, Ross Formation, Ireland. In: Nilsen, T. H., Shew, R. D., Steffens, G. S. and Studlick, J. R. J. (Eds). Atlas of Deep-Water Outcrops. AAPG Studies in Geology 56: 201-205.

Chapin, M. A. 2007. Sheets and incised channels of the Kilcloher Cliff section, Ross Formation, Ireland. In: Nilsen, T. H., Shew, R. D., Steffens, G. S. and Studlick, J. R. J. (Eds). Atlas of Deep-Water Outcrops. AAPG Studies in Geology 56: 196-200.

Chapin, M. A. and Keller, F. B. 2007. Channel-fill sandstones at San Clemente State Beach, California, USA. In: Nilsen, T. H., Shew, R. D., Steffens, G. S. and Studlick, J. R. J. (Eds). Atlas of Deep-Water Outcrops. AAPG Studies in Geology 56: 401-405.

Clark, J. & Gardiner, A. 2000, "Outcrop analogues for deep-water channel and levee genetic units from the Grès d'Annot turbidite system, SE France", *Deep-Water Reservoirs of the World. Gulf Coast Section-SEPM Twentieth Annual Research Conference, Proceedings, SEPM, Houston*SEPM, , pp. 175.

Clark, J., Stanbrook, D. & Gardiner, A. 2007, "Architecture and facies of confined deep-water clastics in the Grand Coyer Remnant, Gres d'Annot, France", *Atlas of deep-water outcrops: AAPG Studies in Geology,* vol. 56, pp. 174-180.

Clark, Julian D., and Kevin T. Pickering. 1996 "Architectural elements and growth patterns of submarine channels: application to hydrocarbon exploration." AAPG bulletin 80.2: 194-220.

Clifton, H.E. 1984, "Sedimentation units in stratified resedimented conglomerate, Paleocene submarine canyon fill, Point Lobos, California", .

Colella, A. and Di Geronimo, I. 1987. Surface sediments and macrofaunas of the Crati submarine fan (Ionian Sea, Italy). Sedimentary Geology 51(3-4): 257-277.

Cronin, B., Celik, H. & Hurst, A. 2007, "Sinuous channels in late stages of entrenched deep-water channel complexes, Hasret Mountain Main Channel, Turkey", *Atlas of deep-water outcrops: AAPG Studies in Geology,* vol. 56, pp. 368-372.

Cross, N.E., Cunningham, A., Cook, R.J., Taha, A., Esmaie, E. & El Swidan, N. 2009, "Three-dimensional seismic geomorphology of a deep-water slope-channel system: The Sequoia field, offshore west Nile Delta, Egypt", *AAPG Bulletin,* vol. 93, no. 8, pp. 1063-1086.

Daly, R.A. 1936, "Origin of submarine canyons", *American Journal of Science,* , no. 186, pp. 401-420.

Deptuck, M.E., Steffens, G.S., Barton, M. & Pirmez, C. 2003, "Architecture and evolution of upper fan channel-belts on the Niger Delta slope and in the Arabian Sea", *Marine and Petroleum Geology,* vol. 20, no. 6, pp. 649-676.

Droz, L., Marsset, T., Ondreas, H., Lopez, M., Savoye, B. and Spy-Anderson, F.-L. 2003. Architecture of an active mud-rich turbidite system; the Zaire Fan (Congo-Angola margin Southeast Atlantic); results from ZaiAngo 1 and 2 cruises. AAPG Bulletin 87(7): 1145-1168.

Dykstra, M. & Kneller, B. 2007, "Canyon San Fernando, Mexico: a deep-water, channel-levee complex exhibiting evolution from submarine canyon—confined to unconfined", *Atlas of deep-water outcrops: AAPG Studies in Geology,* vol. 56, pp. 226-230.

Ercilla, G., Alonso, B. & Baraza, J. 2000, "High resolution morpho-sedimentary characteristics of the distal Orinoco turbidite system", *Deep-water reservoirs of the world: Gulf Coast Section SEPM 20th Annual Research Conference*SEPM, , pp. 374.

Eschard, R., Albouy, E., Deschamps, R., Euzen, T. & Ayub, A. 2003, "Downstream evolution of turbiditic channel complexes in the Pab Range outcrops (Maastrichtian, Pakistan)", *Marine and Petroleum Geology,* vol. 20, no. 6, pp. 691-710.

Etienne, S., Mulder, T., Razin, P., Bez, M., Désaubliaux, G., Joussiaume, R. & Tournadour, E. 2013, "Proximal to distal turbiditic sheet-sand heterogeneities: Characteristics of associated internal channels. Examples from the Trois Evêchés area, Eocene-Oligocene Annot Sandstones (Grès d'Annot), SE France", *Marine and Petroleum Geology,* vol. 41, pp. 117-133.

Euzen, T., Eschard, R. and Albouy, E. 2007. Stratigraphic architecture of a channel complex in the midfan setting of the Lower Pab Basin Floor Fan, North Baddho Dhora, Pakistan. In: Nilsen, T. H., Shew, R. D., Steffens, G. S. and Studlick, J. R. J. (Eds). Atlas of Deep-Water Outcrops. AAPG Studies in Geology 56: 290-294.

Ezz, H., Cantelli, A. & Imran, J. 2014, "A Polynomial Model for Lateral Thickness Decay of Submarine Channel–Levees", *Journal of Sedimentary Research,* vol. 84, no. 1, pp. 51-57.

Ezz, Hesham, Alessandro Cantelli, and Jasim Imran. 2014 "A Polynomial Model for Lateral Thickness Decay of Submarine Channel–Levees." Journal of Sedimentary Research 84.1: 51-57.

Flint, S., Hodgson, D., Sixsmith, P., Grecula, M. & Wickens, H. "DeV., 2007, Deepwater basin floor/slope deposits of the Laingsburg Depocenter, Karoo Basin, South Africa", *Atlas of Deepwater Outcrops, American Association of Petroleum Geologists, ST56,* , pp. 326-329.

Gammon, P. R., Arnott, R. W. C. and Ross, G. M. 2007. Architectural relationships between channels, levees, and debris flows: Isaac channel 6, Castle Creek South, Lower Isaac Formation, Windermere Supergroup, British Columbia, Canada. In: Nilsen, T. H., Shew, R. D., Steffens, G. S. and Studlick, J. R. J. (Eds). Atlas of Deep-Water Outcrops. AAPG Studies in Geology 56: 102-105.

Gardner, M.H. & Borer, J.M. 2000, "Submarine channel architecture along a slope to basin profile, Brushy Canyon Formation, West Texas", *SPECIAL PUBLICATION-SEPM,* vol. 68, pp. 195-214.

Gardner, Michael H., and James M. Borer. 2000 "Submarine channel architecture along a slope to basin profile, Brushy Canyon Formation, West Texas."SPECIAL PUBLICATION-SEPM 68: 195-214.

Grecula, M., Flint, S., Potts, G., Wickens, D. & Johnson, S. 2003, "Partial ponding of turbidite systems in a basin with subtle growth-fold topography: Laingsburg-Karoo, South Africa", *Journal of Sedimentary Research,* vol. 73, no. 4, pp. 603-620.

Grecula, M., Flint, S.S., Wickens, H.D.V. & Johnson, S.D. 2003, "Upward-thickening patterns and lateral continuity of Permian sand-rich turbidite channel fills, Laingsburg Karoo, South Africa", *Sedimentology,* vol. 50, no. 5, pp. 831-853.

Habgood, E.L., Kenyon, N.H., Masson, D.G., Akhmetzhanov, A., Weaver, P.P., Gardner, J. & Mulder, T. 2003, "Deep-water sediment wave fields, bottom current sand channels and gravity flow channel-lobe systems: Gulf of Cadiz, NE Atlantic", *Sedimentology,* vol. 50, no. 3, pp. 483-510.

Hickson, T.A. & Lowe, D.R. 2002, "Facies architecture of a submarine fan channel–levee complex: the Juniper Ridge Conglomerate, Coalinga, California", *Sedimentology,* vol. 49, no. 2, pp. 335-362.

Hodgson, D. M., Drinkwater, N. J., Flint, S. S., Luthi, S. M., Hodgetts, D., Johannessen, E. P., Wickens, H. d. V., Keogh, K. J., Kavanagh, J. P. and Howell, J. A. (2007). Fine-grained, submarine-fan growth and the distribution of lithofacies and architectural elements: an example (Fan 4) from the Skoorsteenberg Formation Basin, South Africa. In: Nilsen, T. H., Shew, R. D., Steffens, G. S. and Studlick, J. R. J. (Eds). Atlas of Deep-Water Outcrops. AAPG Studies in Geology 56: 322-325.

Hofsta, M. 2012. On bidisperse grain size distributions in high density turbidity currents.

Hubbard, S.M., Romans, B.W. & Graham, S.A. 2007, "34Deep-water Channel Margin Architecture, Cerro Toro Formation, Cerro Mocho, Chile", .

Hübscher, C., Spieβ, V., Breitzke, M. & Weber, M.E. 1997, "The youngest channel-levee system of the Bengal Fan: Results from digital sediment echosounder data", *Marine Geology,* vol. 141, no. 1, pp. 125-145.

Hurst, A., Verstralen, I., Cronin, B. & Hartley, A. 1999, "Sand-rich fairways in deep-water clastic reservoirs: genetic units, capturing uncertainty, and a new approach to reservoir modeling", *AAPG Bulletin,* vol. 83, no. 7, pp. 1096-1118.

Imran, Jasim, Gary Parker, and Nikolaos Katopodes. 1998 "A numerical model of channel inception on submarine fans." Journal of Geophysical Research: Oceans (1978–2012) 103.C1: 1219-1238.

Johnson, C. G., et al. 2012 "Grain-size segregation and levee formation in geophysical mass flows." Journal of Geophysical Research: Earth Surface (2003–2012) 117.F1.

Joseph, P., Babonneau, N., Bourgeois, A., Guillocheau, F. & Seguin, J. 2007, "Stratigraphic architecture, seismic and dynamic signature of a sand-rich turbidite ramp: Cime Dieu de Delfy, Grès d'Annot Formation, France", *Atlas of deep-water outcrops.,* .

Kirschner, R.H. & Bouma, A.H. 2000, "Characteristics of a distributary channel-levee-overbank system, Tanqua Karoo", *SPECIAL PUBLICATION-SEPM,* vol. 68, pp. 233-244.

Kostaschuk, R. A., Luternauer, J. L., McKenna, G. T. and Moslow, T. F. 1992. Sediment transport in a submarine channel system; Fraser River delta, Canada. Journal of Sedimentary Petrology 62(2): 273-282.

Kuenen, P.H. 1966, "Matrix of turbidites: experimental approach", *Sedimentology,* vol. 7, no. 4, pp. 267-297.

Laurin, J., Wallace, K., Arnott, R. & Schwarz, E. 2007, "31Stratigraphic Anatomy and Depositional History of Complex, Isaac Formation, Windermere Supergroup, British Columbia, Canada", .

Leeder, M.R. 2009, *Sedimentology and sedimentary basins: from turbulence to tectonics,* John Wiley & Sons.

Lien, T., Walker, R.G. & Martinsen, O.J. 2003, "Turbidites in the Upper Carboniferous Ross Formation, western Ireland: reconstruction of a channel and spillover system", *Sedimentology,* vol. 50, no. 1, pp. 113-148.

Lomas, S.A. 1999, "A Lower Cretaceous clastic slope succession, Livingston Island, Antarctica: sand-body characteristics, depositional processes and implications for slope apron depositional models", *Sedimentology,* vol. 46, no. 3, pp. 477-504.

Maier, Katherine L., et al. 2013 "Deep-sea channel evolution and stratigraphic architecture from inception to abandonment from high-resolution Autonomous Underwater Vehicle surveys offshore central California." Sedimentology 60.4: 935-960.

Martinsen, O. & Lien, T. 2007, "Contrasting styles of slope deposition in the Gull Island Formation, Ireland", *Atlas of Deep-Water Outcrops, American Association of Petroleum Geologists, Studies in Geology,* vol. 56, pp. 210-214.

McHargue, Tim, et al. 2011 "Architecture of turbidite channel systems on the continental slope: patterns and predictions." Marine and Petroleum Geology28.3: 728-743.

Meiburg, E. & Kneller, B. 2010, "Turbidity currents and their deposits", *Annual Review of Fluid Mechanics,* vol. 42, pp. 135-156.

Michielsen, P. 2014. Turbidity current linked to level composition.

Middleton, G.V. 1966, "Experiments on density and turbidity currents: I. Motion of the head", *Canadian Journal of Earth Sciences,* vol. 3, no. 4, pp. 523-546.

Middleton, G.V. 1993, "Sediment deposition from turbidity currents", *Annual Review of Earth and Planetary Sciences,* vol. 21, pp. 89-114.

Moslow, T.F. 2000, "Reservoir architecture of a fine-grained turbidite system: Lower Triassic Montney Formation, Western Canada Sedimentary Basin", *Deep-water Reservoirs of the World, Conference Proceedings, Gulf Coast SEPM. P. Weimer, RM Slatt, J. Coleman, NC Rosen, H. Nelson, AH Bouma, MJ Styzen, and DT Lawrence (eds.)*SEPM, , pp. 686.

Mutti, E. 1979, "Turbidites et cones sous-marins profonds", *Sédimentation détritique (fluviatile, littorale et marine),* vol. 1, pp. 353-419.

Nakajima, T. & Kneller, B.C. 2013, "Quantitative analysis of the geometry of submarine external levees", *Sedimentology,* vol. 60, no. 4, pp. 877-910.

Nakajima, Takeshi, and Benjamin C. Kneller. 2013 "Quantitative analysis of the geometry of submarine external levees." Sedimentology 60.4: 877-910.

Navarro, L., Khan, Z. & Arnott, R. 2007, "Architecture of a deep-water channel-levee complex: Channel 3, Castle Creek South, Isaac Formation, Windermere Supergroup, British Columbia, Canada", *Atlas of deep-water outcrops: AAPG Studies in Geology,* vol. 56, pp. 93-96.

Nilsen, T. H., Steffens, G. S. and Prather, B. E. 2007. Conglomeratic channels, Brockie Lake, Idaho, USA. In: Nilsen, T. H., Shew, R. D., Steffens, G. S. and Studlick, J. R. J. (Eds). Atlas of Deep-Water Outcrops. AAPG Studies in Geology 56: 406-410.

Nilsen, T.H., Shew, R.D., Steffens, G.S. & Studlick, J. 2008, *Atlas of Deep-Water Outcrops: AAPG Studies in Geology 56,* AAPG.

Normark, W., Piper, D. & Hiscott, R. 1998, "Sea level controls on the textural characteristics and depositional architecture of the Hueneme and associated submarine fan systems, Santa Monica Basin, California", *Sedimentology,* vol. 45, no. 1, pp. 53-70.

Ó Cofaigh, C., Dowdeswell, J.A. & Kenyon, N.H. 2006, "Geophysical investigations of a high-latitude submarine channel system and associated channel-mouth lobe in the Lofoten Basin, Polar North Atlantic", *Marine Geology,* vol. 226, no. 1, pp. 41-50.

O'byrne, C., Prather, B., Pirmez, C., Barton, M. & Steffens, G. 2007, "Coarse-grained bar forms in the condor channel complex, Cerro Toro Formation at Lago Sarmiento, Chile", *Atlas of Deep-Water Outcrops, American Association of Petroleum Geologists, Studies in Geology,* vol. 56, pp. 154-156.

O'Byrne, C., Prather, B., Sylvester, Z., Pirmez, C., Couzens, B., Smith, R., Barton, M., Steffens, G. & Willson, J. 2007, "Architecture of a Deep-water Levee Avulsion, Silla Ojo Mesa, Parque Nacional Torres del Paine, Chile", *Deep-water Outcrops of the World Atlas: AAPG, Studies in Geology,* vol. 56, pp. 143e147.

O'Byrne, C. J., Barton, M. D., Prather, B., Pirmez, C., Sylvester, Z., Commins, D. and Coffa, A. 2007. Deep-water channel-complex architectures, Popo Fault Block, Brushy Canyon Formation, Texas, USA - Part 1: stratal framework. In: Nilsen, T. H., Shew, R. D., Steffens, G. S. and Studlick, J. R. J. (Eds). Atlas of Deep-Water Outcrops. AAPG Studies in Geology 56: 457-462.

O'Byrne, C., Barton, M., Steffens, G., Pirmez, C. & Buergisser, H. 2007, "Architecture of a laterally migrating channel complex: Channel 4, Isaac Formation, Windermere Supergroup, Castle Creek North, British Columbia, Canada", *Atlas of Deep-Water Outcrops, American Association of Petroleum Geologists, Studies in Geology,* vol. 56, pp. 115-118.

Parker, G., Garcia, M., Fukushima, Y. & Yu, W. 1987, "Experiments on turbidity currents over an erodible bed", *Journal of Hydraulic Research,* vol. 25, no. 1, pp. 123-147.

Piper, D., Hiscott, R. & Normark, W. 1999, "Outcrop-scale acoustic facies analysis and latest Quaternary development of Hueneme and Dume submarine fans, offshore California", *Sedimentology,* vol. 46, no. 1, pp. 47-78.

Pirmez, C. & Imran, J. 2003, "Reconstruction of turbidity currents in Amazon Channel", *Marine and Petroleum Geology,* vol. 20, no. 6, pp. 823-849.

Plink-Bjorklund, P. and Steel, R. 2007. Type II shelf margin, Hogsnyta, Norway: attached slope turbidite system. In: Nilsen, T. H., Shew, R. D., Steffens, G. S. and Studlick, J. R. J. (Eds). Atlas of Deep-Water Outcrops. AAPG Studies in Geology 56: 282-286.

Prins, M., Postma, G., Cleveringa, J., Cramp, A. & Kenyon, N. 2000, "Controls on terrigenous sediment supply to the Arabian Sea during the late Quaternary: the Indus Fan", *Marine Geology,* vol. 169, no. 3, pp. 327-349.

Prior, D. B. and Bornhold, B. D. 1989. Submarine sedimentation on a developing Holocene fan delta. Sedimentology 36(6): 1053-1076.

Pyles, D. & Slatt, R. 2007, "Stratigraphy of the Lewis Shale, Wyoming, USA, applications to understanding shelf edge to base-of-slope changes in stratigraphic architecture of prograding basin margins", *Atlas of Deep-Water Outcrops: American Association of Petroleum Geologists,* vol. 56.

Pyles, D.R. 2007, "Architectural elements in a ponded submarine fan, Carboniferous Ross Sandstone, western Ireland", *Atlas of deep-water outcrops: AAPG Studies in Geology,* vol. 56, pp. 206-209.

Pyles, D.R., Jennette, D.C., Tomasso, M., Beaubouef, R.T. & Rossen, C. 2010, "Concepts learned from a 3D outcrop of a sinuous slope channel complex: Beacon Channel Complex, Brushy Canyon Formation, West Texas, USA", *Journal of Sedimentary Research,* vol. 80, no. 1, pp. 67-96.

Roscoe, R. 1953, "Suspensions", *Flow Properties of Disperse Systems,* , pp. 1-38.

Rossen, C. & Beaubouef, R. 2007, "Slope-channel complexes at Guadalupe Canyon, Upper Brushy Canyon Formation, Texas, USA", *Atlas of deep-water outcrops: AAPG Studies in Geology,* vol. 56, pp. 429-431.

Rossen, C. & Beaubouef, R. 2007, "Toe-of-slope channel complexes at Buena Vista, Upper Brushy Canyon Formation, Texas, USA", *Atlas of deep-water outcrops: AAPG Studies in Geology,* vol. 56, pp. 450-456.

Rowland, Joel C., George E. Hilley, and Andrea Fildani. 2010 "A test of initiation of submarine leveed channels by deposition alone." Journal of Sedimentary Research 80.8: 710-727.

Satur, N., Hurst, A., Kelling, G., Cronin, B. & Gürbüz, K. 2007, "89Components of Feeder Systems to Cingöz Formation at Karaisali, Turkey", .

Schwarz, E. & Arnott, R. 2007, "Stratigraphic and depositional architecture of a slope channel system: Isaac Channel 5, Castle Creek South, Isaac Formation, Windermere Supergroup, British Columbia, Canada", *Atlas of Deep-Water Outcrops, American Association of Petroleum Geologists, Studies in Geology,* vol. 56, pp. 97-101.

Schwarz, Ernesto, and R. William C. Arnott. 2007 "Anatomy and evolution of a slope channel-complex set (Neoproterozoic Isaac Formation, Windermere Supergroup, southern Canadian Cordillera): implications for reservoir characterization." Journal of Sedimentary Research 77.2: 89-109.

Schwenk, T., Spieß, V., Breitzke, M. & Hübscher, C. 2005, "The architecture and evolution of the Middle Bengal Fan in vicinity of the active channel–levee system imaged by high-resolution seismic data", *Marine and Petroleum Geology,* vol. 22, no. 5, pp. 637-656.

Shew, R. D. 2007. Channel architectures and associated facies in the Brushy Canyon and Cherry Canyon Formations, Guadalupe Mountains area, Texas, USA. In: Nilsen, T. H., Shew, R. D., Steffens, G. S. and Studlick, J. R. J. (Eds). Atlas of Deep-Water Outcrops. AAPG Studies in Geology 56: 475-484.

Simpson, J.E. 1999, *Gravity currents: In the environment and the laboratory,* Cambridge University Press.

Sinclair, H. 2000, "Delta-fed turbidites infilling topographically complex basins: a new depositional model for the Annot Sandstones, SE France", *Journal of Sedimentary Research,* vol. 70, no. 3, pp. 504-519.

Slatt, R., Minken, J., Van Dyke, S., Pyles, D., Witten, A. & Young, R. 2007, "Scales of heterogeneity of an outcropping leveed-channel system, Cretaceous Dad Sandstone Member, Lewis Shale, Wyoming, USA", *Atlas of Deep-Water Outcrops, American Association of Petroleum Geologists, Studies in Geology,* vol. 56.

Soreghan, M.J., Scholz, C.A. & Wells, J.T. 1999, "Coarse-grained, deep-water sedimentation along a border fault margin of Lake Malawi, Africa: seismic stratigraphic analysis", *Journal of Sedimentary Research,* vol. 69, no. 4.

Steel, R., Plink-Bjorklund, P. and Mellere, D. 2007. Storvola, Type 1 shelf margin, Norway. In: Nilsen, T. H., Shew, R. D., Steffens, G. S. and Studlick, J. R. J. (Eds). Atlas of Deep-Water Outcrops. AAPG Studies in Geology 56: 274-281.

Straub, K.M., Mohrig, D., McElroy, B., Buttles, J. & Pirmez, C. 2008, "Interactions between turbidity currents and topography in aggrading sinuous submarine channels: A laboratory study", *Geological Society of America Bulletin,* vol. 120, no. 3-4, pp. 368-385.

Straub, Kyle M., and David Mohrig. 2008 "Quantifying the morphology and growth of levees in aggrading submarine channels." Journal of Geophysical Research: Earth Surface (2003–2012) 113.F3.

Struss, I., Blisniuk, P., Brandes, C., Kischkies, M. and Winsemann, J. 2007.Channel geometries and internal deformation patterns of the Playa Las Tablas channel-levee system, Nicaragua. In: Nilsen, T. H., Shew, R. D., Steffens, G. S. and Studlick, J. R. J. (Eds). Atlas of Deep-Water Outcrops. AAPG Studies in Geology 56: 265-267.

Struss, I., Brandes, C., Vandre, C. and Winsemann, J. 2007. Lithofacies and depositional architecture of an upper fan channel complex, Punta Naranjo, Nicaragua. In: Nilsen, T. H., Shew, R. D., Steffens, G. S. and Studlick, J. R. J. (Eds). Atlas of Deep-Water Outcrops. AAPG Studies in Geology 56: 268-270.

Teng, L.S. & Gorsline, D.S. 1989, "Late Cenozoic sedimentation in California Continental Borderland basins as revealed by seismic facies analysis", *Geological Society of America Bulletin,* vol. 101, no. 1, pp. 27-41.

Torres, J., Droz, L., Savoye, B., Terentieva, E., Cochonat, P., Kenyon, N. & Canals, M. 1997, "Deep-sea avulsion and morphosedimentary evolution of the Rhône Fan Valley and Neofan

during the Late Quaternary (north-western Mediterranean Sea)", *Sedimentology,* vol. 44, no. 3, pp. 457-477.

Trincardi, F., Correggiari, A., Field, M. & Normark, W. 1995, "Turbidite Deposition From Multiple Sources: Quaternary Paola Basin Eeastern Tyrrhenian Sea)", *Journal of Sedimentary Research,* vol. 65, no. 4.

Valente, A., Cavuoto, G., Nardi, G. & Martelli, L. 2007, "Miocene channel-fill deposits, Tempa della Pantanella, Italy", *Atlas of deep-water outcrops: AAPG Studies in Geology,* vol. 56, pp. 218-221.

Vedder, J. 1987, "Regional geology and petroleum potential of the southern California borderland".

Walker, R.G. & Mutti, E. 1973, "Part IV. Turbidite Facies and Facies Associations", .

Xu, J., Noble, M. & Rosenfeld, L.K. 2004, "In-situ measurements of velocity structure within turbidity currents", *Geophysical Research Letters,* vol. 31, no. 9.

Zeng, J., Lowe, D. R., Prior, D. B., Wiseman, W. J. r. and Bornhold, B. D. 1991. Flow properties of turbidity currents in Bute Inlet, British Columbia. Sedimentology 38(6): 975-996.

Appendix A

This appendix contains the digital elevation models of the unsuccessful runs. The models were roughly processed as they were not further used in this study.

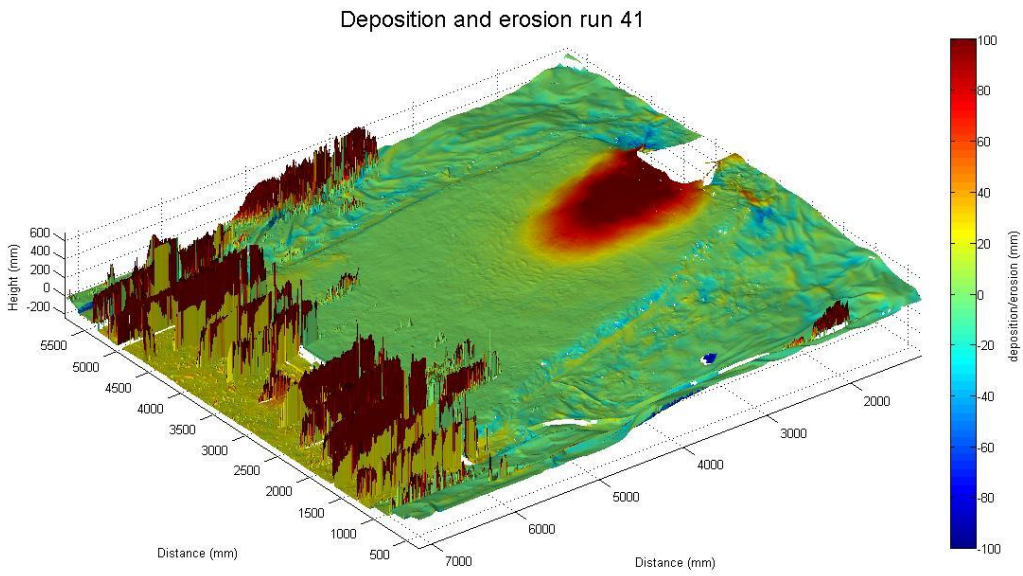

Figure 36: Digital elevation model of run 41.

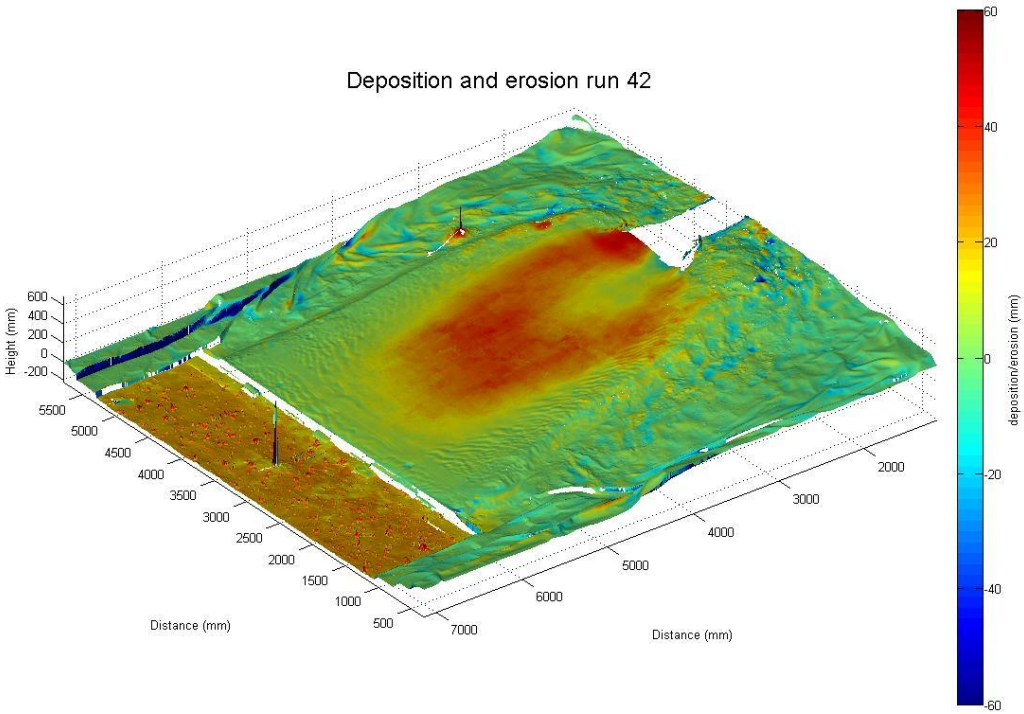

Figure 37: Digital elevation model of run 42.

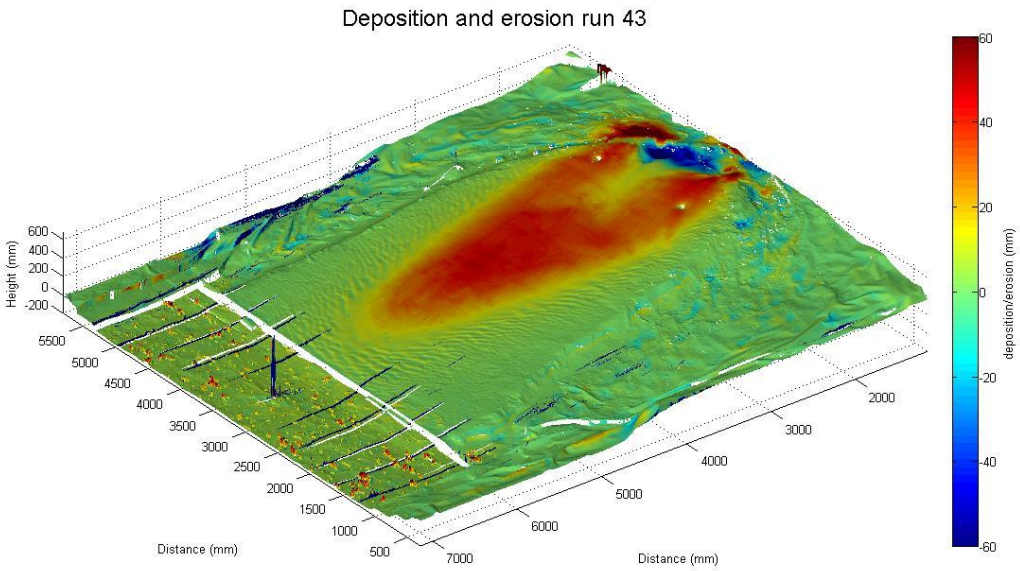

Figure 38: Digital elevation model of run 43.

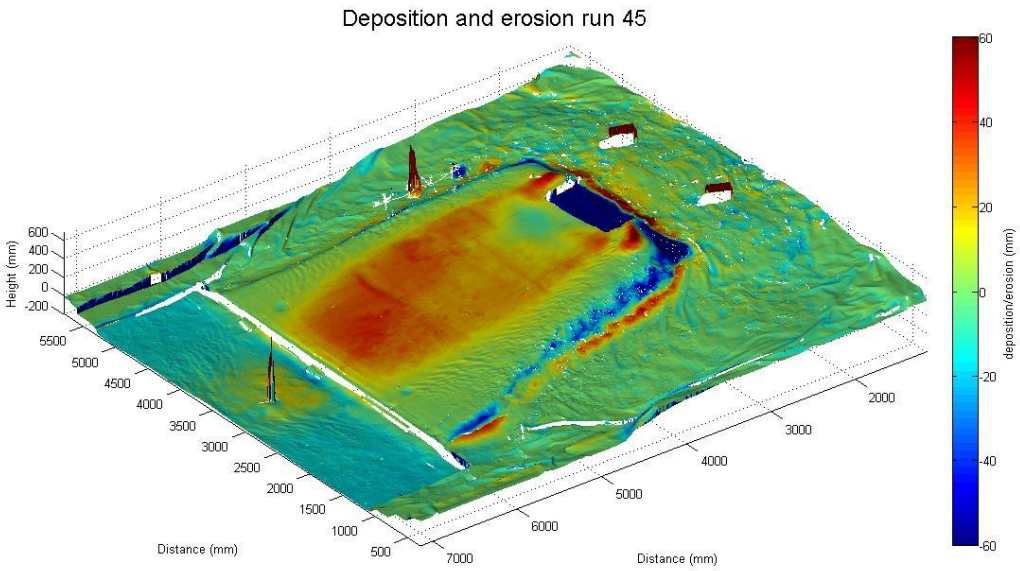

Figure 39: Digital elevation model of run 45.

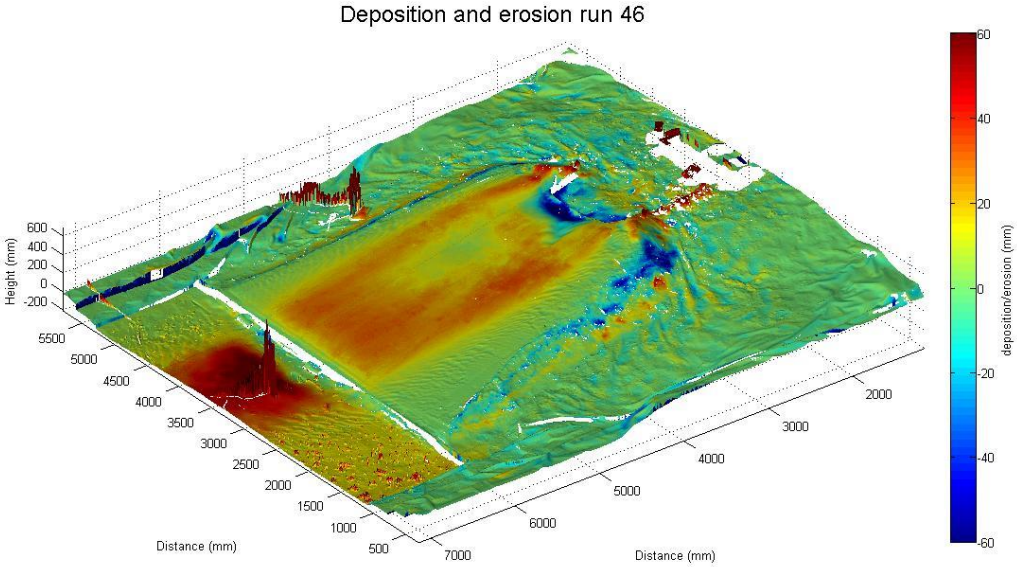

Figure 40: Digital elevation model of run 46.

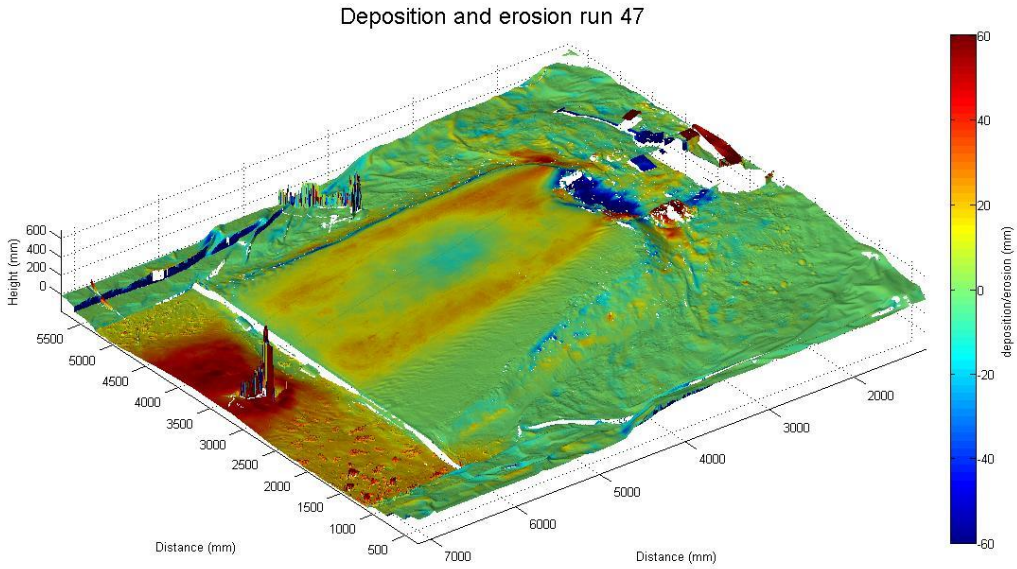

Figure 41: Digital elevation model of run 47.

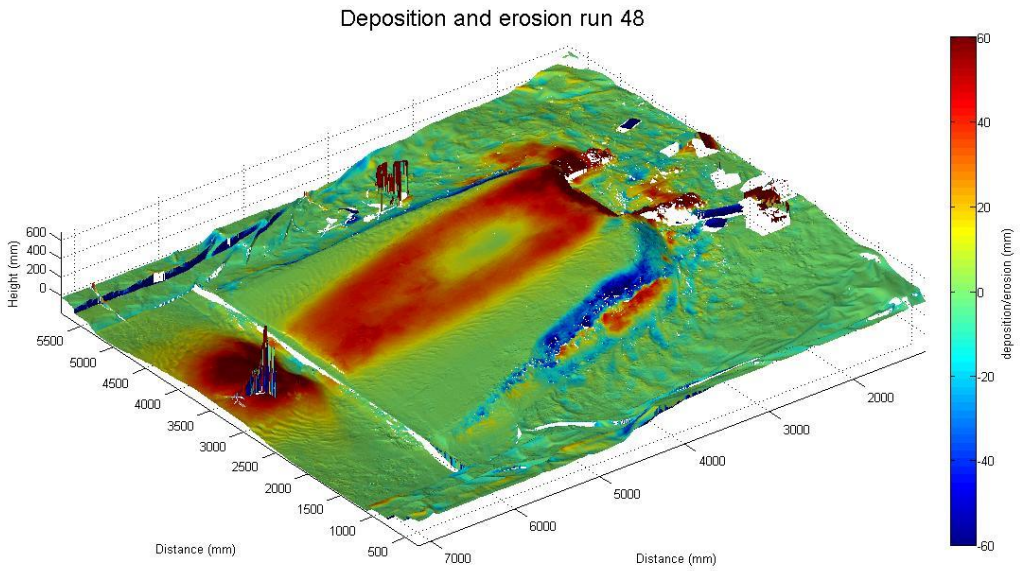

Figure 42: Digital elevation model of run 48.